AGU PUBLICATIONS

Geochemistry, Geophysics, Geosystems

RESEARCH ARTICLE
10.1002/2015GC005798

Key Points:
- Pore water geochemistry at two seismogenic areas is discussed
- Carbonate dissolution process has been identified
- Link between seismic activity in Marmara Sea and pore water changes is discussed

Correspondence to:
R. Livio,
livio.ruffine@ifremer.fr

Citation:
Ruffine, L., et al. (2015), Pore water geochemistry at two seismogenic areas in the Sea of Marmara, *Geochem. Geophys. Geosyst.*, *16*, 2038–2057, doi:10.1002/2015GC005798.

Received 27 FEB 2015
Accepted 30 MAY 2015
Accepted article online 3 JUN 2015
Published online 2 JUL 2015

Pore water geochemistry at two seismogenic areas in the Sea of Marmara

Livio Ruffine[1], Yoan Germain[1], Alina Polonia[2], Alexis de Prunelé[1], Claire Croguennec[1], Jean-Pierre Donval[1], Mathilde Pitel-Roudaut[1], Emmanuel Ponzevera[1], Jean-Claude Caprais[3], Christophe Brandily[3], Céline Grall[1,4,5], Claire Bollinger[6], Louis Géli[1], and Luca Gasperini[2]

[1]IFREMER, Département REM, Unité des Géosciences Marines, 29280 Plouzané, France, [2]Istituto di Scienze Marine—Geologia Marina, Consiglio Nazionale delle Ricerche, IT-40129 Bologna, Italy, [3]IFREMER, Département REM, Unité des Ecosystémes et Environnements Profonds, 29280 Plouzané, France, [4]CEREGE, Collège de France, CNRS—Aix Marseille University, F-13545 Aix-en-Provence, France, [5]Lamont-Doherty Earth Observatory of Columbia University, P.O. Box 1000, Palisades, NY 10964, USA, [6]Institut Universitaire Européenne Bretagne, UBO, CNRS, UMR 6538, 29280 Plouzané, France

Abstract Within the Sea of Marmara, the highly active North Anatolian Fault (NAF) is responsible for major earthquakes (Mw $\geq$ 7), and acts as a pathway for fluid migration from deep sources to the seafloor. This work reports on pore water geochemistry from three sediment cores collected in the Gulfs of Izmit and Gemlik, along the Northern and the Middle strands of the NAF, respectively. The resulting data set shows that anaerobic oxidation of methane (AOM) is the major process responsible for sulfate depletion in the shallow sediment. In the Gulf of Gemlik, depth concentration profiles of both sulfate and alkalinity exhibit a kink-type profile. The Sulfate Methane Transition Zone (SMTZ) is located at moderate depth in the area. In the Gulf of Izmit, the low concentrations observed near the seawater-sediment interface for sulfate, calcium, strontium, and magnesium result from rapid geochemical processes, AOM, and carbonate precipitation, occurring in the uppermost part of the sedimentary column and sustained by free methane accumulation. Barite dissolution and carbonate recrystallization have also been identified at deeper depth at the eastern-most basin of the Gulf of Izmit. This is supported by the profile of the strontium isotope ratios ($^{87}Sr/^{86}Sr$) as a function of depth which exhibits negative anomalies compared to the modern seawater value. The strontium isotopic signature also shows that these carbonates had precipitated during the reconnection of the Sea of Marmara with the Mediterranean Sea. Finally, a first attempt to interpret the sulfate profiles observed in the light of the seismic activity at both sites is presented. We propose the hypothesis that seismic activity in the areas is responsible for the transient sulfate profile, and that the very shallow SMTZ depths observed in the Gulf of Izmit is likely due to episodic release of significant amount of methane.

1. Introduction

For the purpose of risk assessment and monitoring of earthquakes in both Turkey and the Southern Europe, the Sea of Marmara (SoM) has been the subject of numerous investigations over the last decade. The main reason is because it is cut lengthwise by the North Anatolian Fault, a continental transform fault which accommodates 20–27 mm/yr of right-lateral motion between the Anatolian and Eurasian plates [*Hergert and Heidbach*, 2011; *Hergert et al*., 2011; *Le Pichon et al*., 2003; *Meade et al*., 2002; *Reilinger et al*., 2006]. This fault has caused devastating earthquakes during historical times, resulting from the rupture of several of its segments [*Ambraseys*, 2000, 2001, 2002; *Ambraseys and Jackson*, 2000; *Armijo et al*., 2005; *Barka*, 1999; *Barka et al*., 2002; *Gasperini et al*., 2011; *Hubert-Ferrari et al*., 2000; *Kuscu et al*., 2009, 2005; *Langridge et al*., 2002; *Le Pichon et al*., 2001; *Sengor et al*., 2005; *Ucarkus et al*., 2011]. Seismic hazard in the area is particularly high and deserves particular attention in this densely populated region that plays an important role in the economy of the country.

The Sea of Marmara is also characterized by a large number of widespread gas expulsion sites at the seafloor, bubbling up to several tens to hundreds of meters into the water column [*Burnard et al*., 2012; *Dupré et al*., 2010; *Gasperini et al*., 2012; *Géli et al*., 2008; *Kuscu et al*., 2005; *Tary et al*., 2012; *Zitter et al*., 2008]. Such gases are primarily of thermogenic origin in the western Marmara, which is geologically connected to the hydrocarbon reservoirs of the Thrace basin, while mainly biogenic gases, i.e., generated by microbial activity, have been collected from the seafloor of the Cinarcik Basin and the Gulf of Izmit (Figure 1) [*Bourry et al*., 2009;

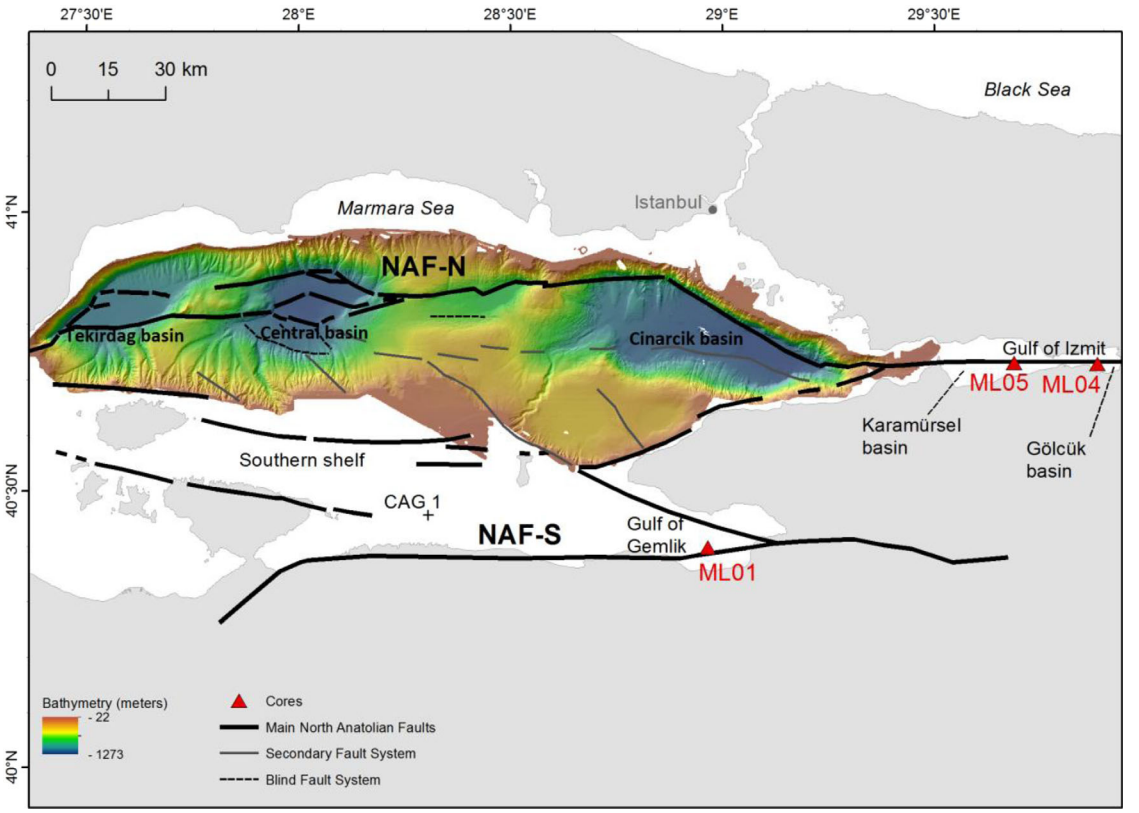

Figure 1. Location map of the study area.

Gasperini et al., 2012; *Kuscu et al.*, 2005; *Ruffine et al.*, 2012]. The chemical composition of pore waters is also very heterogeneous from one site to another [*Burnard et al.*, 2012; *Cagatay et al.*, 2004; *Halbach et al.*, 2004; *Tryon et al.*, 2010]. The observed distribution of gases in the shallow sediments may result from the mixing of distinct sources at different depths, and might be controlled by the tectonic activity, in, at least two ways: (1) formation of pathways for fluid migration due to the presence of conduits formed by faulting along the NAF principal deformation zone, whose permeability is controlled by the stress status; (2) remobilization of sediments and gas eventually trapped within the sedimentary sequence as a consequence of seismic shaking or mass wasting induced by major earthquakes. These geologic peculiarities make the Sea of Marmara an interesting observation site for studying relationships between tectonics and fluid migration, and to investigate the potential of gas and fluid emission sites along active faults with the aim of monitoring seismic activity before, during and after large magnitude earthquakes. A recent long-term monitoring experiment carried out close to the eastern termination of the 1999 Mw = 7.4 Izmit earthquake has confirmed the potential of combining seismological and gas-geochemical observations of the seafloor to study the seismic cycle [*Embriaco et al.*, 2014]. Previous studies of the water column in the Sea of Marmara have shown a systematic association between fluid expulsion sites along the North Anatolian Fault and the fault network, and the basin edges [*Dupré et al.*, 2010; *Kuscu et al.*, 2005, 2008]. Thus, those faults play an important role in the migration of deep-sourced fluids to the seafloor. Accordingly, the inception, intensity, and/or lifetime of these created fluid seeps and plumes may be strongly influenced by the fault activity and seismic events [*Cormier et al.*, 2006; *Kuscu et al.*, 2005, 2008]. In this context, several questions arise. How does the seismic cycle along each NAF segment influence the fluid migration pattern? Or, in other words, are there any systematic differences in the chemistry of pore waters between recently ruptured segments and segments already sealed after a large earthquake? Does microseismicity influence the "normal" emission of gas and fluid to the seafloor? Previous studies carried out in different parts of the SoM [*Çağatay et al.*, 2012; *Gasperini et al.*, 2011; *Gasperini et al.*, 2012; *McHugh et al.*, 2006] attempted to address these questions without providing an ultimate answer.

In this paper, we present the first study on pore water chemistry at two distinct segments of the North Anatolian Fault within the Gulf of Gemlik (GoG) and the Gulf of Izmit (GoI). These gulfs are characterized by similar tectonic settings but different situations relative to their stress regime. In fact, while the Gulf of Izmit underwent a recent surface rupture due to the 1999 Mw = 7.4 Izmit earthquake, the Gulf of Gemlik did not undergo large magnitude events in recent times (see next section). One specific question discussed here is whether the sulfate profiles and the recorded seismic activity of these two areas are linked. Such an approach has already been considered in previous work. *Halbach et al*. [2004] were the first ones who related the transient sulfate profile to tectonic events in the Sea of Marmara. *Fischer et al*. [2013] move further with this approach and showed that subduction zone earthquake can potentially trigger hydrocarbon seepage which depletes pore water sulfate via the anaerobic oxidation of methane. From a completely different geological setting, *Noethen and Kasten* [2011] measured similar types of sulfate profile when investigating methane hydrate-bearing settings offshore Congo. They claimed that such profiles reflect sudden change in the methane fluxes. Here this question regarding the link between sulfate profile and the seismic activity will be explored by investigating three cores recovered during the MARMARA-2010 Scientific Cruise on board the *R/V* Urania.

2. Geological Settings

2.1. Seismotectonic Settings

The North Anatolian Fault splits into three main branches, the north, the middle, and the south branches before reaching the Sea of Marmara [*Barka*, 1992]. The northern branch enters in the eastern SoM through the Gulf of Izmit (Figure 1), forming a 50 km long E-W oriented gulf along this segment and comprising three basins separated by two sills [*Barka and Kadinsky-Cade*, 1988; *Goeruer et al*., 1997; *Kuscu et al*., 2002]. This branch forms a right-lateral step-over [*Gasperini et al*., 2011], where en échelon normal faults are responsible for subsidence within the gulf. The middle branch enters in the southern shelf of the Sea of Marmara through the GoG. Estimated slip rate suggests that the northern branch accommodates the major part of the slip, between 60 and 80% of the total motion, while the middle and the southern branches between 20 and 40% of the total motion [*Ergintav et al*., 2009; *Gasperini et al*., 2011; *Hearn et al*., 2009; *Hergert and Heidbach*, 2010].

Earthquake historical catalogs suggest that the last major earthquakes occurred along the middle NAF branch in 1419, 1855, and 1863 [*Ambraseys*, 2000, 2001; *Ambraseys*, 2006; *Ambraseys*, 2006; *Barka*, 1999; *Gasperini et al*., 2011; *Gok and Polat*, 2012; *Gorur and Cagatay*, 2010; *Karabulut et al*., 2011; *Pondrelli et al*., 2011; *Tanircan and Savas*, 2011; *Yalciner et al*., 2002]. Seismological data suggest that a moderate earthquake ($M_w = 5.2$) occurred along this fault segment in 24 October 2006 [*Irmak et al*., 2007; *Pondrelli et al*., 2011]. Conversely, the GoI was struck by a large magnitude earthquake in 1999 ($M_w = 7.4$) that caused the rupture of the entire Izmit fault segment [*Armijo et al*., 2005; *Çağatay et al*., 2012; *Cakir et al*., 2003; *Gasperini et al*., 2011, 2012]. In this area, images of gas-charged sediments [*Gasperini et al*., 2012; *Kuscu et al*., 2002, 2005], polygonal cracks on the basin floor, black sulfide-like sediment patches, and mud volcanoes [*Gasperini et al*., 2012] suggest that sudden fluid release and sediment fluidization have occurred during this large earthquake.

2.2. Paleoenvironmental Context

During the last glacial period, the main paleo-shoreline of the Sea of Marmara was at 85 m below the present-day sea level, and underwent oscillation between 95 and 105 m below the present-day sea level before the Holocene [*Cagatay et al*., 2004, 2009; *Eris et al*., 2011; *McHugh et al*., 2006]. This level is ubiquitous in the Sea of Marmara, and coincides with the sill depth of the Dardanelles. In the Gulf of Gemlik, chirp subbottom echo sounder profiles and core correlation suggest that during the last glacial maximum it was a basin characterized by a freshwater environment, most probably separated by the main Marmara basin by a −38 m deep sill. During this lacustrine phase, the eastern GoG was occupied by a prograding delta [*Gasperini et al*., 2011]. The Holocene marine transgression led to the abandoning of this delta, which was dated through the study of a sediment core at ≈11 kyr BP [*Gasperini et al*., 2011]. The frontal lobe of the Gemlik lacustrine delta was used as a piercing point to estimate the strike-slip rate along the NAF middle strand at 4 ± 0.4 mm/yr [*Gasperini et al*., 2011]. In the Karamürsel basin (Figure 1), the Younger Drias paleoshoreline has been drawn at −65 m [*Cagatay et al*., 2003; *Cormier et al*., 2006; *Eris et al*., 2007], suggesting

Table 1. Coordinates of the Studied Cores

Core Name	Coordinates (Lat.; Long.)
ML01	40,3978016; 28,967134
ML04	40,7281494; 29,8857973
ML05	40,7303827; 29,6890688

that the central part of this small basin was submerged by lacustrine water during the last glacial maximum and that marine incursion occurred earlier in this basin relative to the eastern Gölcük basin. Finally, in the western Gulf of Izmit (the Darica Basin, Figure 1), a paleo-shoreline located −85 m before the present-day datum was studied by *Polonia et al*. [2004]. The presence of this feature, abandoned 10,200 ± 50 years B.P. and a river channel displaced by the North Anatolian Fault northern strand in the Gulf of Izmit allowed for a slip-rate estimate of 10 mm/yr during the Holocene [*Polonia et al*., 2004].

3. Sampling and Methods

3.1. Water Sampling and Analytical Methods

Bottom water samples were collected from CTD-rosette hydrocast for major and minor element analyses. Three gravity cores were taken for pore water sampling, one in the Gulf of Gemlik (ML01, at 113 m water depth) and two in the Gulf of Izmit (ML 04 and ML05, at 37 and 209 m water depth, respectively, Figure 1). Coring close to the fault relies on the accuracy allowed for the position system onboard the *R/V* Urania, which was ±1 m. Such an accuracy on the positioning of the coring station was achieved in three ways: (1) the DGPS antenna was virtually placed on the vertical of the coring cable, thus eliminating the offset due to the finite distance between the antenna and the coring winch; (2) the corer was launched for its latest 15/20 m of free-fall only when the inclinometer placed on top of the cable indicates the perfect vertical (±some decimal degrees); (3) the chirp sonar system pinging was turned on while coring, and in the shallow waters investigated here, it was possible to see on the recording the corer reaching the bottom. This also enabled us to compare the stratigraphy of the planned station with that of the "real" station.

Sediment cores were collected using a 1.2 metric tons gravity corer. In order to preserve the core top, and taking advantage from the softness of the sediments, the corer was operated without trigger and at a relatively low speed of penetration. Radioisotopes measurements carried out on twin cores for marine paleosesimology studies confirm that the core loss is negligible, and the sedimentary sequence is complete and includes sediments as young as at least 1999 [*Cagatay et al*., 2012]. Sampled core coordinates are presented in Table 1.

After retrieval, the cores were cut into 1 m segments and subsequently transferred to a chemical laboratory onboard *R/V* Urania. Pore water was extracted using Rhyzon sampler. The latter consists of a hydrophilic, porous polymer tube with 2.5 mm in diameter and 50 mm in length [*Seeberg-Elverfeldt et al*., 2005]. Rhyzons were inserted into the sediment at a depth resolution of 20 or 30 cm. Immediately after sampling, 1 mL aliquot of sample was used for total alkalinity (Alk) measurements. This was performed by direct titration with ultrapure 0.1 N HCl from a potentiometric tritrator 848 Tritrino Plus from Metrohm®. The remaining sample volume was stored in 6 mL preevacuated vials and frozen for further analyses onshore.

Methane concentrations were measured by headspace gas chromatography, with an instrument Perichrom 2100 equipped with a flame ionization detector connected to a headspace injector (Dani HSS 86.50), while stable carbon isotopic ratio of methane ($\delta^{13}C_{-CH4}$) was determined with a *G2201-i* CRDS analyzer from Picarro. The average analytical precision was of 4% and 0.9‰, for methane concentration and $\delta^{13}C_{-CH4}$, respectively.

Major elements were analyzed using a Dionex® ICS-2000 instrument equipped with an autosampler at the Laboratoire de Géochimie et Métallogénie, Unité des Geosciences Marines, IFREMER. Anions (sulfate and chloride) were analyzed on an Ionpac AS-17C column of 250 mm in length and 4 mm in diameter equipped with a 4 mm ASRS suppressor. The detection limits were 1.5 and 5 ppm for sulfate and chloride, respectively. Major cations (magnesium and calcium) were analyzed on an Ionpac CS-12A column of 250 mm in length and 4 mm in diameter equipped with a CAES suppressor. The detection limit was 0.1 ppm for both species. All elements were quantified by comparing their peak intensity with equivalently diluted International Association for Physical Sciences of Oceans (IAPSO) standard seawater. The latter was analyzed at the beginning of each run. The estimated accuracy was within ±3% of the mole fraction for all ions.

Concentrations of pore water minor elements (strontium and barium) were determined by Inductively Coupled Plasma Mass-Spectrometry with High Resolution to avoid ionic interference (ICP-MS HR). The analyses were carried out with an instrument from Thermo Scientific at the Pôle Spectrométrique Ocean, PSO (a joint analytical lab between Ifremer-UBO-CNRS). Pore waters were diluted at 1/25 with 2% Nitric Acid ULTREX II Ultrapure Reagent (J.T. Baker, Phillipsburg, NJ, USA), in a clean lab. Both NASS-5 Seawater Reference Material for Trace Metals and monoelemental PlasmaCAL standards (SCP Science, Québec, Canada) were used for calibration purpose. The overall estimated accuracy was within ±4% of the mole fraction for all ions.

Strontium isotope-ratio measurements ($^{87}Sr/^{86}Sr$) were carried out using a Neptune Multiple Collector Inductively Coupled Plasma Mass-Spectrometer (MC-ICP-MS) from Thermo Scientific at the PSO. A sample volume of 125 μL was taken and mixed up with 1 mL of nitric acid 5 N in a SAVILLEX beaker. The latter was evaporated on a hotplate at 373 K overnight. The residual phase was reacidified with 0.5 mL of nitric acid 3 N, and then loaded onto a column containing a preconditioned crown-ether cation exchange resin Sr Spec (EICHROM, Bruz, France). The resin was previously washed with 2 mL of purified water (Milli-Q, 18.2 MΩ cm), then 1 mL of nitric acid 3 N. The elution was done with 2.5 mL of nitric acid 3 N and then the strontium collection with 4 mL of nitric acid 0.01 N, followed by 1 mL of purified water. After an evaporation step, the solid-state sample was dissolved in 0.5 nitric acid at 2% (w/w). The results were normalized using the NIST SRM-987 standard and the obtained values are given with an accuracy better than 0.00004.

3.2. Chirp Profiles Processing

Chirp-sonar profiles were acquired with the 16 transducers, hull mounted BENTHOS (DATASONICS) CHIRP-II profiler, with operating frequencies ranging between 2 and 7 kHz. The pulse duration was selected between 5 and 15 ms, while the trigger rates varied from 0.25 to 0.5 s, depending on water depth. Data were collected using either the time delay or the multiping techniques, insonifying the water column with several chirp-sonar pings. Digital data acquired by the Communication Technology SWANPRO software were recorded in the XTF format on local disks and transferred on the network upon request. Navigation data were made available to the system as lat/long by NMEA sentences of the DGPS receiver at a rate of approximately 1 Hz or by the PDS2000s NMEA at 1 Hz. The XTF data were then converted to SEG-Y using the SeisPrho software [*Gasperini and Stanghellini*, 2009]. The latter was also employed for compiling BMP images of the seismic profiles onboard. Processing and filtering of the data (mainly static correction, gain balancing, swell and noise filtering) was also performed with SeisPrho at the ISMAR laboratories.

3.3. Numerical Modeling of the AOM

The evolution of the Sulfate Methane Transition Zone (SMTZ) with time was simulated using a numerical transport-reaction model, developed in gPROMS software (Process System Enterprise, PSE Ltd). The model expressed the diagenetic equations [*Berner*, 1980; *Boudreau*, 1997], and takes into account the molecular diffusion of methane and sulfate, upward transport of free methane, as well as the rate of Anaerobic Oxidation of Methane (AOM):

$$\theta\frac{\partial[C_i]}{\partial t}=\frac{\partial}{\partial x}\left[\theta\frac{D_i}{\vartheta^2}\frac{\partial[C_i]}{\partial x}\right]+\theta v\frac{\partial[C_i]}{\partial x}-\theta R_{AOM}$$

where t is time (year), θ is the sediment porosity, x is the depth within the sedimentary column (m), ϑ is the sediment tortuosity, C_i and D_i are the concentration (mM) and diffusion coefficient (m^2 yr) of the dissolved species "i," respectively, v is the upward fluid velocity, and R_{AOM} is the reaction rate.

The sediment tortuosity was calculated using Boudreau empirical formulation:

$$\vartheta^2=1-\ln\left(\theta^2\right)$$

The AOM rate was expressed by the following kinetic equation:

$$R_{AOM}=k_{AOM}[SO_4][CH_4]$$

with k_{AOM} is the bimolecular rate constant of the reaction.

Table 2 summarizes the parameters used for the modeling. Chloride was used as conservative species for parameter optimization.

Table 2. Parameters used in the Transport-Reaction Model for the Simulation of the Evolution of the Sulfate Profiles With Time

			Value	
Parameter	Symbol	Unit	ML04	ML05
Model domain	L	m	1	3
Molecular diffusion coefficient, SO_4	D_{SO4}	$m^2\ s^{-1}$	7.86×10^{-10}	7.86×10^{-10}
Molecular diffusion coefficient, CH_4	D_{CH4}	$m^2\ s^{-1}$	1.23×10^{-9}	1.23×10^{-9}
SO_4 concentration at the sediment surface	$[SO_4]$	mM	28.2	28.2
CH_4 concentration at the sediment surface	$[CH_4]$	mM	0	0
CH_4 concentration at lower boundary domain	$[CH_4]$	mM	5.16	27.52
SO_4 flux at lower boundary domain	$\left(\frac{\partial[SO_4]}{\partial x}\right)_L$	$mM\ m^{-1}$	0	0
Upward fluid velocity	v	$cm\ yr^{-1}$	26.7 (for simulation (1)) 2.3 (for simulation (2))	26.7 (for simulation (1)) 2.3 (for simulation (2))
Sediment porosity	θ		0.8	0.8
AOM constant rate	k_{AOM}	$mM^{-1}\ yr^{-1}$	0.126	0.001

4. Results

4.1. Alkalinity, Methane, Major, and Trace Dissolved Elements

The alkalinity and the concentration-depth profiles for chloride, sulfate and methane (both molecular and isotopic), magnesium, calcium, strontium, and barium are shown in Figures 2 and 3. The gray square indicates the bottom water concentration for the dissolved elements. For core ML01 retrieved in the GoG, the chloride profile displays near-constant concentration values close to that of seawater in the upper part, and then a decrease from 612 to 587 m*M* at 230 centimeters below seafloor (cmbsf) to downcore. Dissolved sulfate exhibits a kink-type profile where the concentrations remain nearly constant and close to the seawater value from the seawater-sediment interface over the upper 230 cmbsf, followed by an abrupt change in the gradient as the measured values decrease more rapidly. The alkalinity profile has an opposing trend, with near-constant concentration values until 230 cmbsf, and then an increase with depth. Dissolved methane concentration is low over the entire core, and varies between 0.02 and 1.55 μM. Such low concentrations do not allow for the measurements of $\delta^{13}C_{\text{-CH4}}$. Strontium concentrations are close to that of seawater as well, except at around 130 cmbsf where a peak appears. The latter is likely to be an outlier. Barium concentrations are low as well, with little variations over the full length.

Both cores collected in the Gulf of Izmit display near-seawater chloride concentrations over their full length. It is worth noticing from Figures 2 and 3 that sulfate, calcium, and strontium concentrations at the uppermost part of both Gulf of Izmit cores are abnormally low compared to both the expected seawater values and the measured values at the Gulf of Gemlik.

Sulfate concentration is very low at the uppermost part of core ML04, with a value of 4 m*M* at 15 cmbsf. It decreases to near-zero value at 70 cmbsf. Core ML05 displays a linear decrease with depth and values fall to below the detection limit at 180 cmbsf. Reciprocally, the methane concentrations are very low at the upper part of the cores, and increase significantly from the depth where sulfate is depleted with values up to 296 μM for core ML05. The increase in methane concentration is weaker for core ML04, with values up to 104 μM downcore. $\delta^{13}C_{\text{-CH4}}$ decreases with depth for core ML04 with values ranging from -75.6 to $-59.5‰$, and a minimum at 220 cmbsf where methane concentration starts increasing with depth. For core ML05, $\delta^{13}C_{\text{-CH4}}$ decreases with depth from $-56.7‰$ to $-90.6‰$ at the SMTZ, and then increase to downcore. The alkalinity is characterized by high values even at the uppermost part of both cores, with a maximum around 40,000 μM at the sulfate-depleted depth. Calcium and strontium concentrations increase in the upper 70 cm and then decrease downcore in two steps for core ML04. A gradual decrease is observed for core ML05 in the upper 180 cmbsf to values around 2.3–3.5 m*M* for calcium and 5.6–61 μM for strontium. Constant values are observed downcore for both cores. Core ML04 is characterized by two peaks in barium of 150 and 40 μM at 70 and 220 cmbsf, respectively, whereas near-zero values are observed for core ML05 over its full length.

4.2. Strontium Isotopic Composition

The strontium isotope ratios from pore waters for cores ML01 and ML05 do not show significant depth variations (Figure 4a), and display values of ~0.70915 close to that of modern seawater. For core ML04, the $^{87}Sr/^{86}Sr$

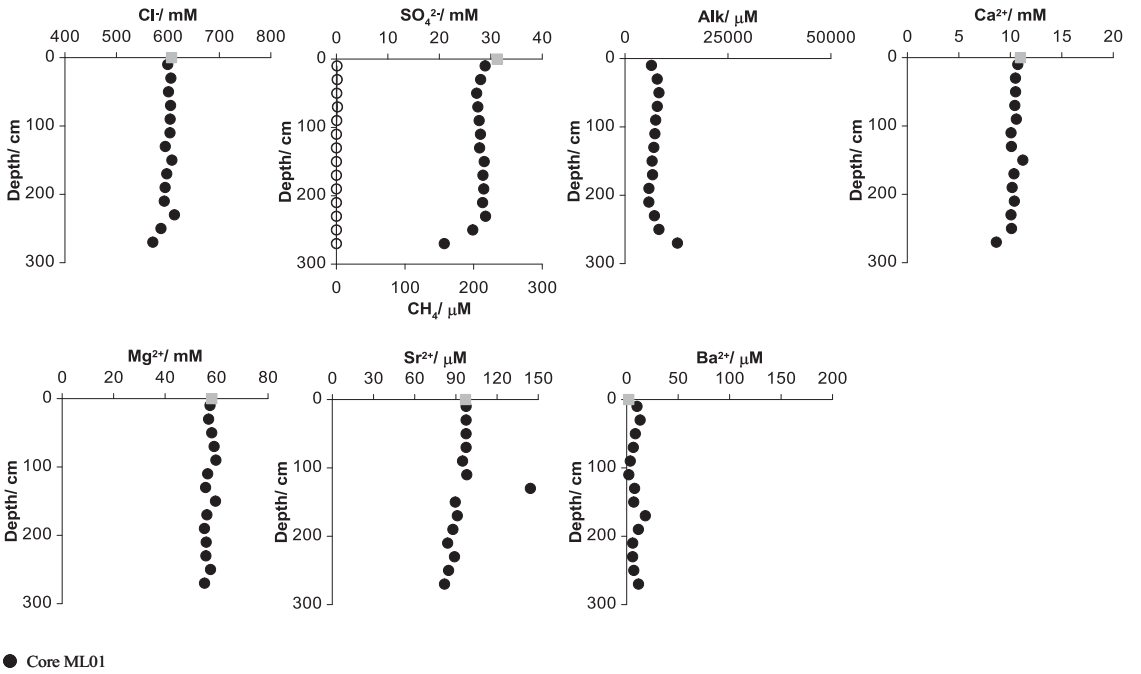

Figure 2. Depth profiles of measured concentrations of dissolved elements for core ML01 recovered in the Gulf of Gemlik.

ratios decrease from 0.70904 at 15 cmbsf to a minimum of 0.70865 at 120 cmbsf, then increase to approach the modern seawater value at 205 cmbsf (Figure 4a) and finally remain relatively constant downcore.

4.3. Geophysical Survey

At each coring station, an accurate interpretation of the chirp-sonar profile was performed both onboard, prior of the coring, to verify the depth and the characteristic of the coring site, and after for an accurate processing. In general, the base of the Holocene in the Sea of Marmara is a clear seismostratigraphic horizon, which is easily followed in high-resolution seismic reflection profiles, due to the high acoustic impedance contrast between the Holocene marine deposits above, and the lacustrine units below. This is particularly true in the shallow water environment, where the marine-lacustrine transition is marked by a ravinement surface or by erosion.

The acoustic waves used to insonify the seafloor and subseafloor, ranging in frequency from 2 to 7 kHz, are scattered by gas bubbles in the water column, showing typical patterns in the records. On the other hand, such acoustic signals used to image the shallow subseafloor are very sensitive to the presence of gas in the sediments, which hamper the penetration and generated the characteristic "blanking" or "blind" windows. All of the selected sampling sites were chosen because: (1) close to the North Anatolian Fault principal deformation zone; (2) close or on top of gas-bearing sediments, as seen by analysis of chirp-sonar profiles; and (3) encompassing a sequence of relative continuous, homogeneous marine sediments, overlapping a lacustrine sequence.

5. Discussion

5.1. Sulfate Consumption and Linked Processes

All three cores have in common a shallow sulfate depletion depth. In anoxic marine sediment, there are two major biogeochemical processes responsible for the sulfate consumption: the mineralization of particulate organic matter and the anaerobic oxidation of methane (AOM) [*Borowski et al*., 1996; *Froelich et al*., 1979; *Meister et al*., 2013; *Niewohner et al*., 1998; *Reeburgh*, 1976; *Regnier et al*., 2011; *Wallmann et al*., 2006a, 2006b]. This paragraph aims at identifying the dominant process affecting the sulfate concentration in the sedimentary column. Previous seismic surveys at both gulfs revealed the presence of gas-charged sediments, and the chemical analysis of gases emanating from the seafloor at different sites showed that

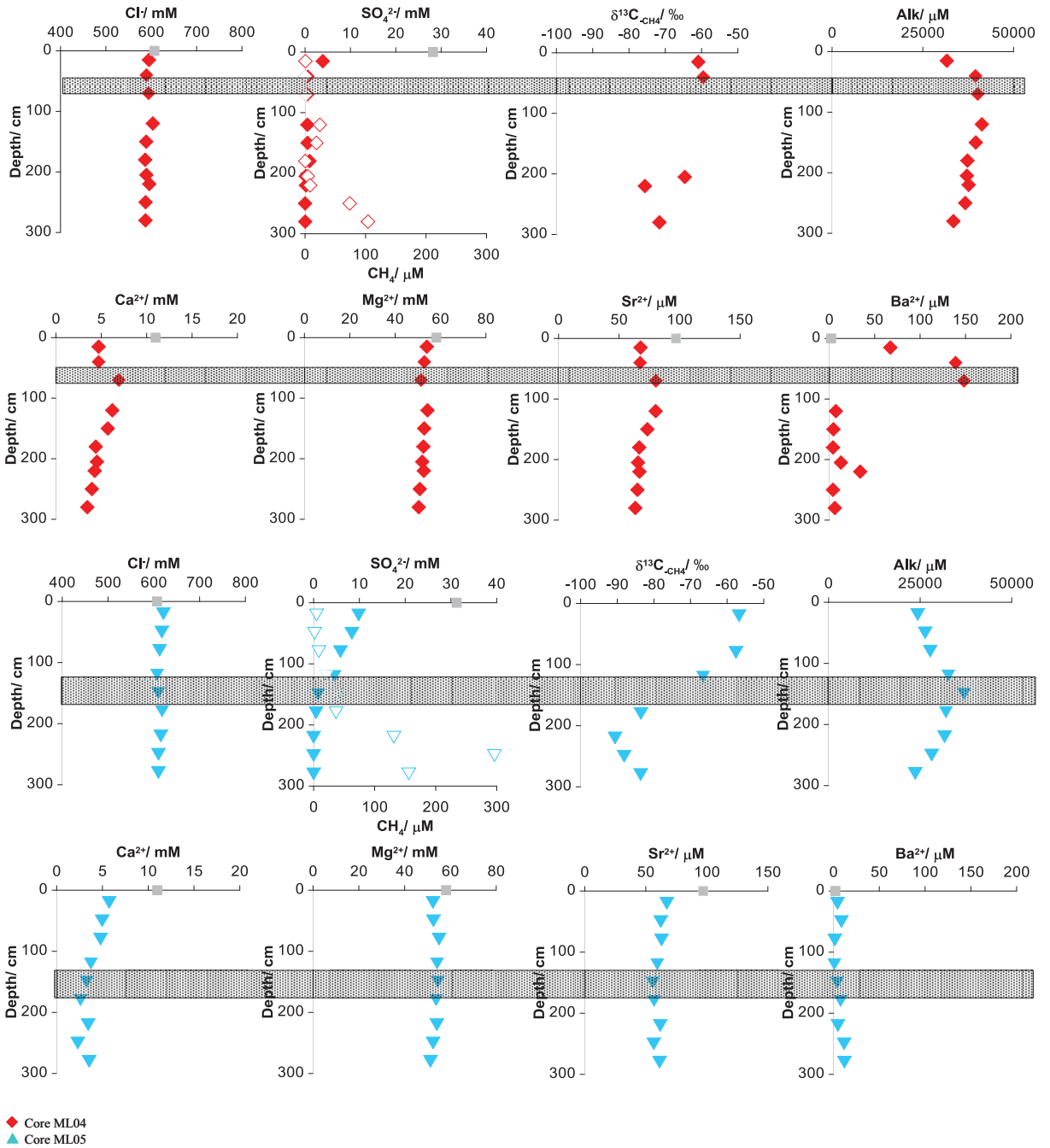

Figure 3. Depth profiles of measured concentrations of dissolved elements and δ^{13}C-CH_4 for cores ML04 and ML05 recovered in the Gulf of Izmit (shaded areas represent the SMTZ intervals, hollow symbol corresponds to methane concentration).

methane is the dominant fraction, especially at the eastern part of the Sea of Marmara [*Bourry et al.*, 2009; *Gasperini et al.*, 2012; *Kuscu et al.*, 2009, 2005]. Figure 5 represents a chirp-sonar profile obtained during the acoustic survey in the Gulf of Gemlik, where core ML01 has been retrieved. It is likely that the base of the Holocene coincides with the clear unconformity at 122 mbsf. However, no stratigraphic constraints are available because our core is well above. The "blindness" of the deposits below such unconformity suggests either the presence of gas or a diagenetic indurated level. In addition, the low methane concentrations together with the absence of a maximum in alkalinity for core ML01 does not allow a direct determination of the process responsible for the sulfate depletion in the GoG. However, the kink-type sulfate profile of

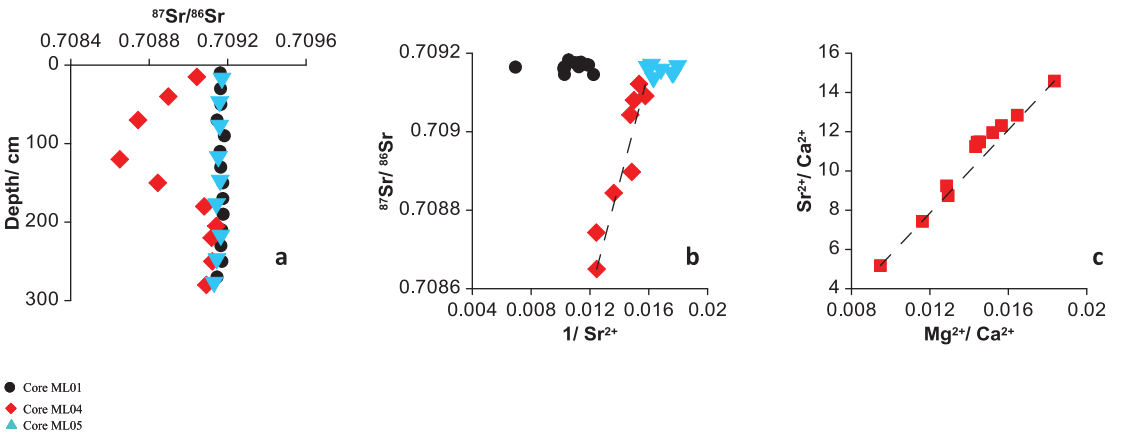

Figure 4. Plots of (a) $^{87}Sr/^{86}Sr$ ratios of the pore fluids as a function of depth, (b) $^{87}Sr/^{86}Sr$ ratios as a function of the reciprocal Sr^{2+} concentration, and (c) Sr^{2+}/Ca^{2+} ratios as a function of Mg^{2+}/Ca^{2+}.

core ML01, characterized by seawater infiltration-simulating concentrations, in combination with the low alkalinity highly suggest that organic matter degradation does not significantly deplete the sulfate pool in the surface sediment at the Gulf of Gemlik. Therefore, it is very likely that AOM is responsible for the sulfate depletion here [*Hong et al*., 2013; *Whiticar*, 1999; *Whiticar and Faber*, 1986], with a supply from the gas-charged sedimentary layer at deeper depth. Thus, the "blindness" observed on Figure 5 is due to gas occurrence. A linear least square regression on the three deepest points gives an estimated Sulfate Methane Transition Zone (SMTZ) shallower than ~360 cmbsf (Figure 6).

For core ML05, the sulfate depletion depth coincides with a maximum in alkalinity, a minimum in $\delta^{13}C_{\text{-CH4}}$ as well as with an increase in methane concentration (Figure 3). The same trends can be observed for core ML04 retrieved in the Gölcük basin except for the depth profile of $\delta^{13}C_{\text{-CH4}}$ which exhibits a minimum at 220 cmbsf. Moreover, the base of the Holocene is around 45 mbsf on the chirp-sonar profile obtained during the acoustic survey at the Gölcük basin where core ML04 has been recovered (Figure 7). We also have evidence of clear erosion due to the fact that this part of the gulf was exposed during the last glacial maximum. Here the pre-Holocene sediments are saturated with gas as revealed by the pore water geochemistry, but no clear evidence of the classical acoustic "blindness" indicative of its occurrence. Nevertheless, gas can easily migrate upward through the NAF which is located at less than 50 m away from the core station and affects the sediment around. Besides, the chirp-sonar profile acquired in the Karamürsel basin (Figure 8) shows a blanking zone below 220 mbsf which clearly indicates the presence of gas saturated sediment.

The combination of all the aforementioned evidence from both geochemistry and geophysics clearly indicates that gas is present within the sedimentary column, and AOM is also responsible for the sulfate depletion in the Gulf of Izmit.

The low $\delta^{13}C_{\text{-CH4}}$ values downcore are indicative of microbial methane generated within the methanogenic zone beneath the SMTZ [*Hong et al*., 2013; *Whiticar*, 1999]. The $\delta^{13}C_{\text{-CH4}}$- depth profiles obtained for the two cores ML04 and ML05 are difference from each other. While core ML05 exhibits a minimum at the SMTZ as commonly seen at methane-seep sites, the minimum value for core ML04 is well below the SMTZ. The overlap between the minimum in $\delta^{13}C_{\text{-CH4}}$ and the SMTZ is due to the carbon isotope equilibration between methane and carbon dioxide [*Yoshinaga et al*., 2014]. This equilibration leads to ^{13}C-rich methane when the sulfate concentration is higher than ~0.5 m*M*, and ^{13}C-depleted methane for lower sulfate concentrations. Here sulfate concentrations are lower than 0.5 m*M* below the SMTZ for both cores. Thus, the lowest $\delta^{13}C_{\text{-CH4}}$ value found at 220 cmbsf for core ML05 likely indicates that the $\delta^{13}C$ equilibration has been reached. It is not the case for core ML04 where the lowest values are located downcore within the methanogenic zone, and thus away from the SMTZ. Such unexpected $\delta^{13}C$ nonbalancing could result from the presence of a residual free methane bypassing the SMTZ. This would influence the equilibration between methane and carbon dioxide, and therefore overprints the $\delta^{13}C$ values of the dissolved methane measured here.

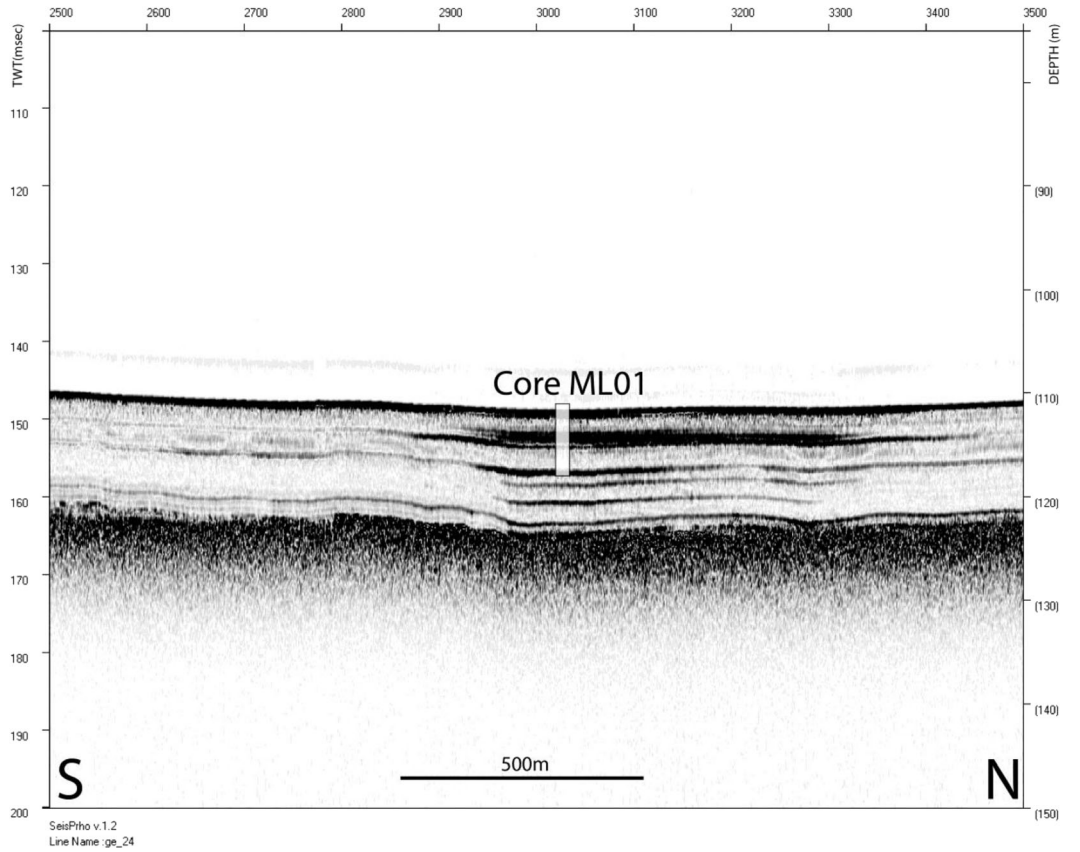

Figure 5. Chirp-sonar profile ge_24 obtained during the acoustic survey at the Gulf of Gemlik. Probably the base of the Holocene coincides with the clear unconformity below −120 m. However, no stratigraphic constraints are available, because the core is well above. The "blindness" of the deposits below such unconformity could suggest either the presence of gas, or a diagenetic, indurated level.

5.2. Process Responsible for the Low Concentration of Sulfate, Calcium, and Magnesium at the Gulf of Izmit

As mentioned previously, the sulfate, calcium, and strontium concentrations at the uppermost part of cores ML04 and ML05 are low. Their values near the sediment-seawater interface are much lower than that of the bottom seawater. Simultaneously, values of alkalinity higher than that expected for seawater are observed at the upper part of both cores. When extrapolating linearly to the seafloor level, the sulfate concentrations obtained are still much lower than the seawater value. Due to our confidence in both the efficiency of the coring and the analyses which have followed, it is unlikely that such low values result from the loss of the upper part of the cores during recovery. One possible explanation is that our spatial resolution for the pore water sampling does not enable us to depict accurately the upper part of the profiles, and therefore we are not able to clearly see rapid processes occurring within this sedimentary interval. This is particularly the case at methane seeps characterized by vigorous emission, where the sulfate depletion occurs at depth lesser than meter scale due to advection of free methane [*Aloisi et al*., 2004a, 2004b; *Lapham et al*., 2008; *Wallmann et al*., 2006a, 2006b; *Wilson et al*., 2014]. Another hypothesis which cannot be discarded owing to the geology of the investigated sites is the loss of the upper part of the sediment due to landslides triggered by the 1999 Izmit earthquake. Evidence of such sedimentary events has already been reported in the area from both

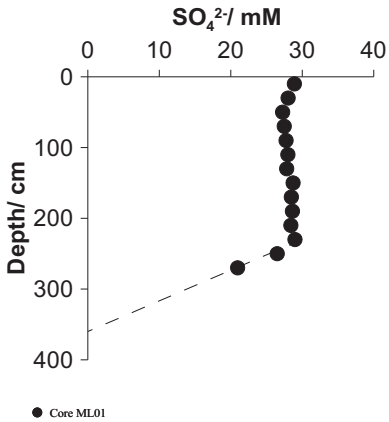

Figure 6. Estimated SMTZ depth obtained by extrapolation.

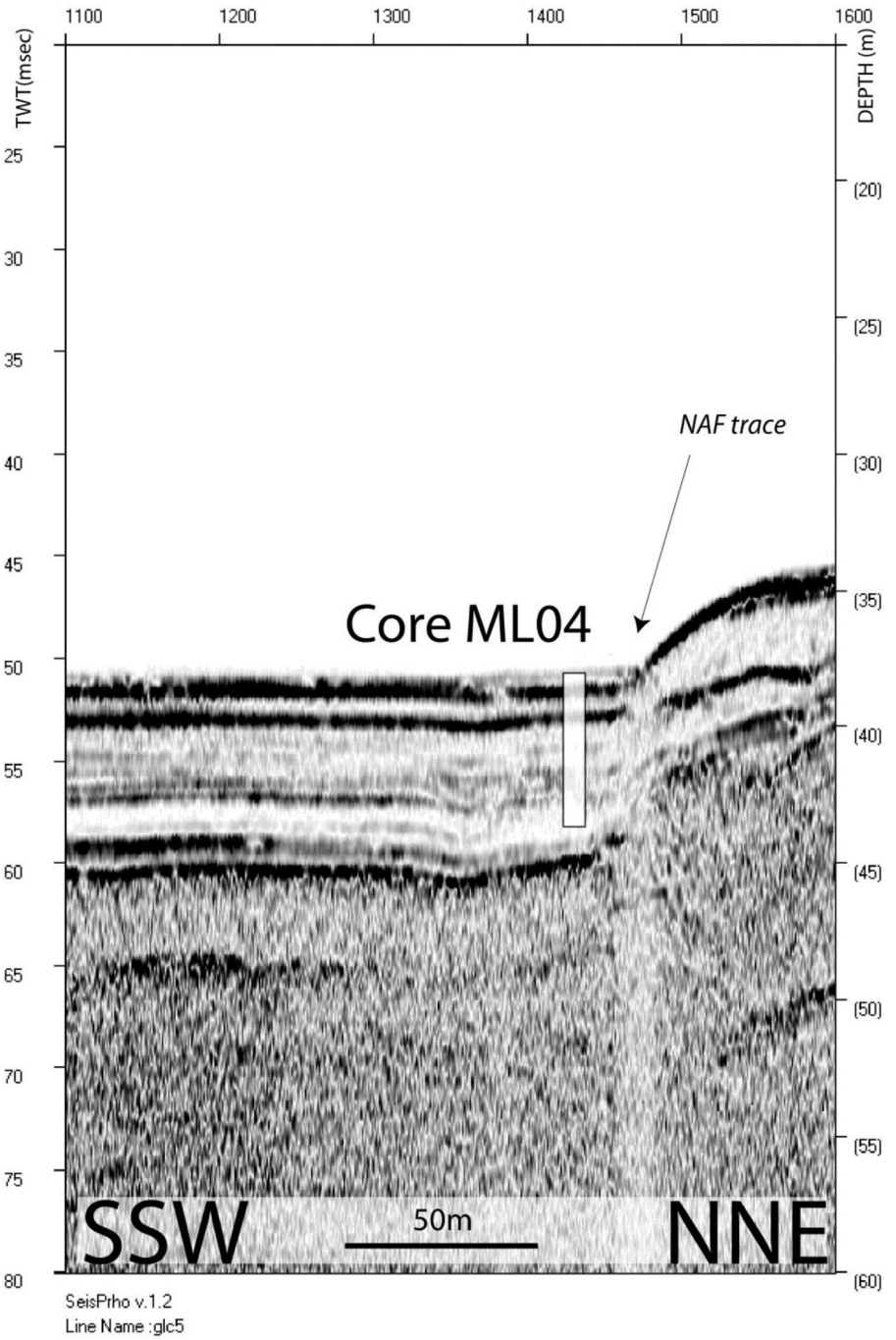

Figure 7. Chirp-sonar profile glc_5 obtained during the acoustic survey at the basin Gölcük (Gulf of Izmit). Base of the Holocene is probably around 60 ms TWT. The preholocene sediments are probably saturated by gas, but no clear evidence of the classical "blind windows" are present.

the study of the sedimentary sequences of collected cores and seismic investigations [*Çağatay et al*., 2012; *Kuscu et al*., 2005]. In fact, *Kuscu et al*. [2005] identified five major zones which have been subject to slumping in the Gölcük basin. Core ML04 is retrieved at one of them, called zone III in their classification. Thus, it may be possible that the sites where the cores ML04 and ML05 have been retrieved have lost the upper part of the sedimentary column, and therefore the upper segment of these element profiles.

In order to test the validity of both hypotheses, we simulated (1) the evolution of the sulfate profile with time after the loss of the upper sedimentary column due to the 1999 Izmit earthquake, and (2) the change

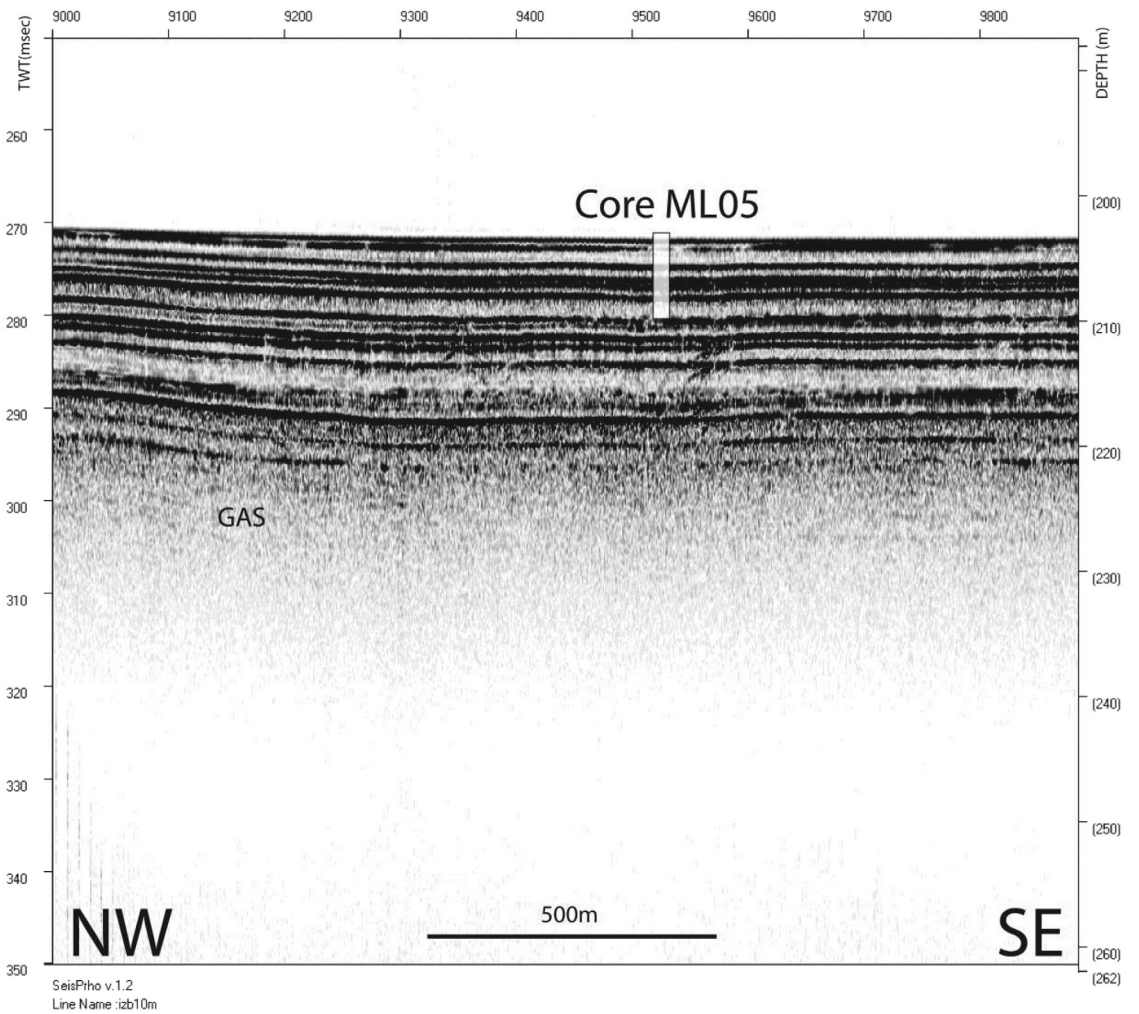

Figure 8. Chirp-sonar profile ibz10m obtained during the acoustic survey at the basin Karamürsel (Gulf of Izmit). The gas saturated sediments are below 220 m, as indicated in the image. Location (to scale) of core ML05 is also indicated.

in the flux of the methane due to episodic gas release moving the AOM reaction zone toward the seafloor. For simulation (1), we assumed that straight after the earthquake-triggered lanslide, the sulfate-free and methane-rich sedimentary column is again in contact with seawater. In simulation (2), the sulfate concentration is taken as the bottom seawater value, and we considered that the upward free methane transport changes from 0 (purely diffisive process) to 26.7 $\pm$ 3 cm yr^{-1}. This value of upward free methane transport has been optimized from previous study carried out by *Halbach et al*. [2004]. The k_{AOM}, which influences the change in the curvature of the profile [*Chuang et al*., 2013], was optimized on the measured sulfate profiles. A constant porosity of 0.80 was taken. For time computing purpose and in order to focus on the sedimentary sequence above the SMTZ, a model length of 1 and 3 m was applied for ML04 and ML05, respectively.

Only the sulfate profile of core ML04 was reasonably reproduced when considering the lost of the upper sedimentary column (Figure 9). For both simulations, best fit was obtained with an upward fluid velocity of 2.3 cm yr^{-1}, which is within the range of the optimized values obtained by *Halbach et al*. [2004]. However, one can clearly see that best fit between the simulation and the measured data is at 6 $\pm$ 1 months after the lost of the sedimentary sequence, and steady state is reached after 21 $\pm$ 2 years. Figure 9 also shows that it was not possible to reproduced the sulfate profile of core ML05 in a reasonable time scale when one considers the scenario of earthquake-triggrered lanslide. Accordingly, the low concentrations of disolved elements observed at the upper part of cores ML04 and ML05 are not the result of the loss of the upper sedimentary column due to the 1999 Izmit earthquake.

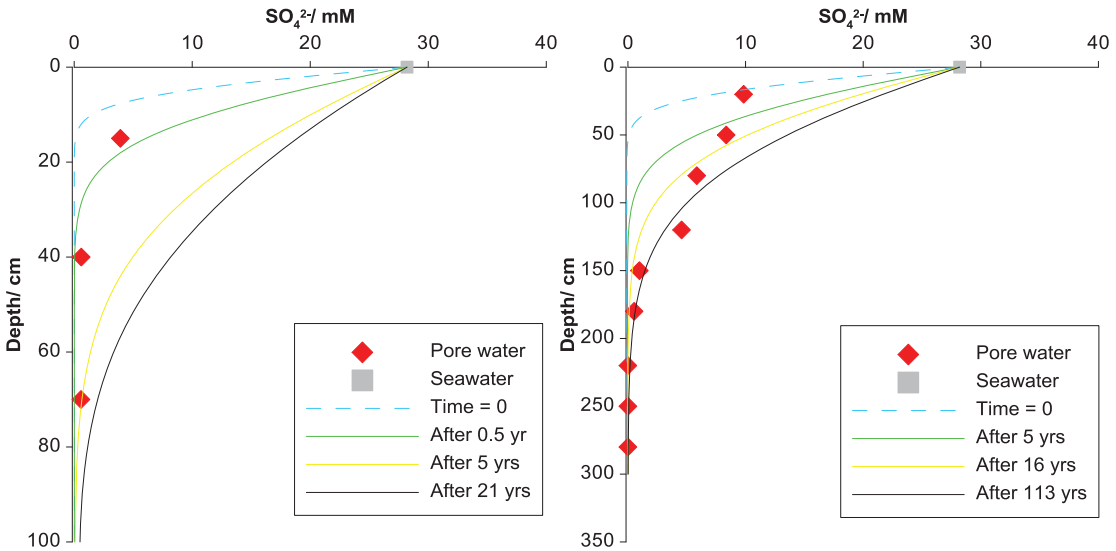

Figure 9. Evolution of the sulfate profile as a function of time for core ML04 and ML05, assuming an earthquake-triggered landslide leading to the loss of the uppermost part of the sedimentary layer.

Conversely, the simulation of a change in the upward free methane transport leads to a good fit of the measured dissolved-sulfate profile for both cores (Figure 10). In this scenario, we assumed a diffisive profile prior to the release of methane gas into the sedimentary column. It would take around 1.5 and 5.5 years for the system to reach present-day profiles for ML04 and ML05, respectively. The return to a new steady state will take around 7 and 13.5 years for ML04 and ML05, respectively. This is also much less than the elapsed time since the 1999 Izmit earthquake. However, this is in agreement with the short time scale for which steady state is reached at methane seeps [*Fischer et al*., 2013]. Although for the starting conditions, we assumed here an absence of upward transport of free methane, a sensivity analysis has shown that the time scale to reach a new steady state after the methane discharge remains in the same order of magnitude for an initial upward methane velocity of 1–2 cm yr^{-1}.

Thus, we believe that the low concentrations observed at the upper part of both cores are the result of rapid geochemical processes consuming sulfate, calcium, and strontium. Moreover, our simulation shows that transient release of methane into the sedimentary column can significantly perturb sulfate profile, and the latter may keep a record of that perturbation decades before the setting up of a new steady state.

5.3. Solid Mineral Phase-Involving Processes

The profiles from Figures 2 and 3 highlight the occurrence of several geochemical reactions as important concentration variations with depth are observed for the pore water elements. These variations reflect the reactivity of the elements at the investigated sedimentary intervals, especially their transfer from or into solid mineral phases. Hence, the following section aims at inferring the occurrence of solid mineral phase-involving processes at both gulfs based on the pore water geochemistry.

5.4. Carbonate-Associated Processes

Aragonite, Mg-calcite, and dolomite are typical authigenic carbonates encountered at cold seep environments [*Baker et al*., 1981; *Bayon et al*., 2007, 2009; *Burton*, 1993; *Burton and Walter*, 1987; *Cangemi et al*., 2010; *Cremiere et al*., 2012; *Feng and Roberts*, 2011; *Feng et al*., 2009; *Himmler et al*., 2010; *Moore et al*., 2004; *Pierre et al*., 2012; *Vanneste et al*., 2012]. They all imply an uptake of bicarbonate, calcium, magnesium, and strontium from the surrounding pore water during their formation; and reciprocally they all release those elements when undergoing a dissolution process. Hence, the evolution of Mg^{2+}/Ca^{2+} and Sr^{2+}/Ca^{2+} ratios in pore waters, solid carbonates, and/or sediments are useful for the identification of the nature of the precipitated carbonate phases [*Bayon et al*., 2007; *Noethen and Kasten*, 2011]. Here we apply the same methodology to our pore water samples in order to get insight into the carbonate-associated processes which take place in the shallow sediment at both gulfs.

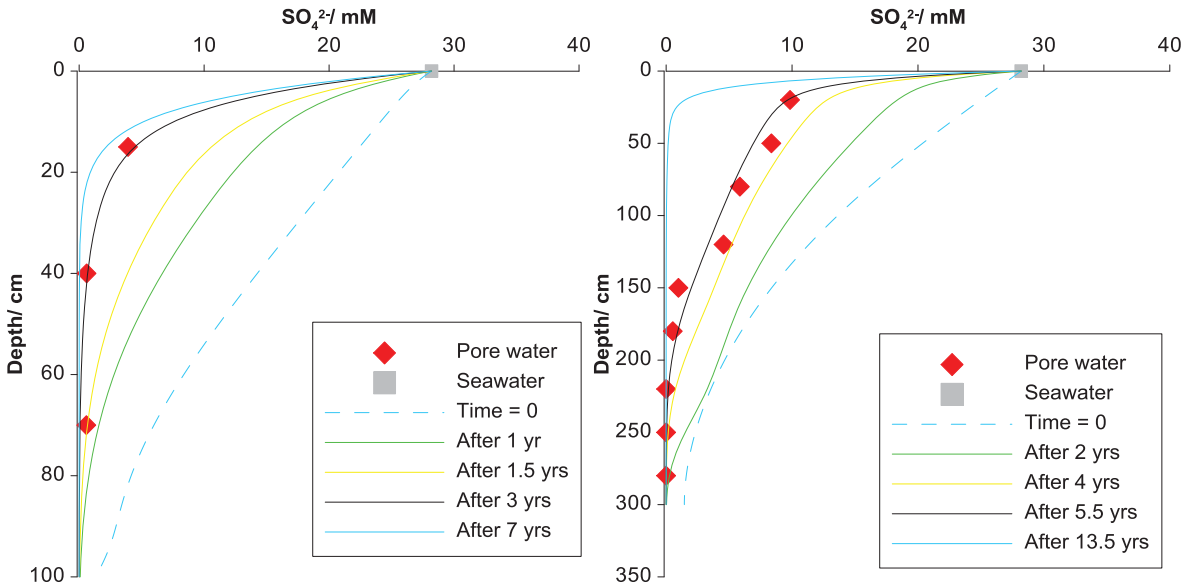

Figure 10. Evolution of the sulfate profile as a function of time after an increase in the upward methane flux for core ML04 and ML05.

Figure 11 represents the depth profiles of Mg^{2+}/Ca^{2+} and Sr^{2+}/Ca^{2+} ratios for the three cores. The profiles from the Gulf of Gemlik site do not show any particular evidence of carbonate-associated processes over its full length. As illustrated in Figure 11, the two cores ML04 and ML05 exhibit different trends although both are characterized by high Mg^{2+}/Ca^{2+} ratios. Within the sediment interval, 70 to ~200 cmbsf core ML04 exhibits Mg^{2+}/Ca^{2+} and Sr^{2+}/Ca^{2+} ratios lower than the uppermost pore water samples. The depth-concentration profiles of these elements show an increase until ~70 or 120 cmbsf, followed by a decrease to ~200 cmbsf (Figure 3). In addition, as mentioned earlier, the $^{87}Sr/^{86}Sr$ versus depth profile displays a source of strontium less radiogenic than that of modern seawater at 120 cmbsf which diffuses downward (Figure 4). Such a profile is generally attributed to carbonate recrystallization at cold seeps [*Scholz et al.*, 2009]. The recrystallization leads to the release of strontium with an isotopic signature characteristic of the fluid from which the carbonates have originally precipitated [*Gieskes et al.*, 1986; *Ussler et al.*, 2000]. This is in agreement with Figures 4b and 4c which represent the $^{87}Sr/^{86}Sr$ ratio as a function of the reciprocal concentrations of Sr and the Mg^{2+}/Ca^{2+} versus Sr^{2+}/Ca^{2+}, respectively. In fact, when considering seawater value and the ratio of 0.70865 (value at the inferred source) as end-members, one can see that all the samples fall onto the dashed mixing line (Figure 4b). Moreover, the minimum value of 0.70865 for the $^{87}Sr/^{86}Sr$ ratio found at 120 cmbsf is very close to that measured on calcite-rich materials (mollusk shells) collected in the Sea of Marmara and which were preserved during the marine water incursion from the Mediterranean Sea [*Vidal et al.*, 2010]. Previous studies have shown that the mixing of the two different water masses, marine water of the Mediterranean Sea and the lacustrine water of the Sea of Marmara, has also promoted the precipitation of carbonates [*Crémière et al.*, 2013; *Reichel and Halbach*, 2007]. Therefore, it is likely that the carbonate layer which is currently undergoing a recrystallization has presumably been formed circa 9 kyr B.P. during the reconnection of the Gölcük basin with the Mediterranean Sea [*Cagatay et al.*, 2003; *Eris et al.*, 2011; *McHugh et al.*, 2008]. In contrast, core ML05 is characterized by an increase of Mg^{2+}/Ca^{2+} and Sr^{2+}/Ca^{2+} ratios down to the SMTZ which is indicative of carbonate precipitation at this sediment horizon.

5.5. Barite Precipitation

At cold seep environments, downward-migrating sulfate-rich seawater reacts with ascending barium-rich fluid to form a barite front just above the SMTZ [*Aloisi et al.*, 2004a, 2004b; *Henkel et al.*, 2012; *Kasten et al.*, 2012; *Snyder et al.*, 2007; *Solomon and Kastner*, 2012]. Upon burial and/or increase in the methane flux, the barite front enters into the sulfate-free zone below the SMTZ and starts to dissociate in order to reach thermodynamic equilibrium with the surrounding pore water. The released barium in turn, diffuses upward and reprecipitates at the subsequently shallower SMTZ horizon which was newly formed. Cores ML01 and ML05 do not show any evidence of barite precipitation as they exhibit low concentrations over their full length

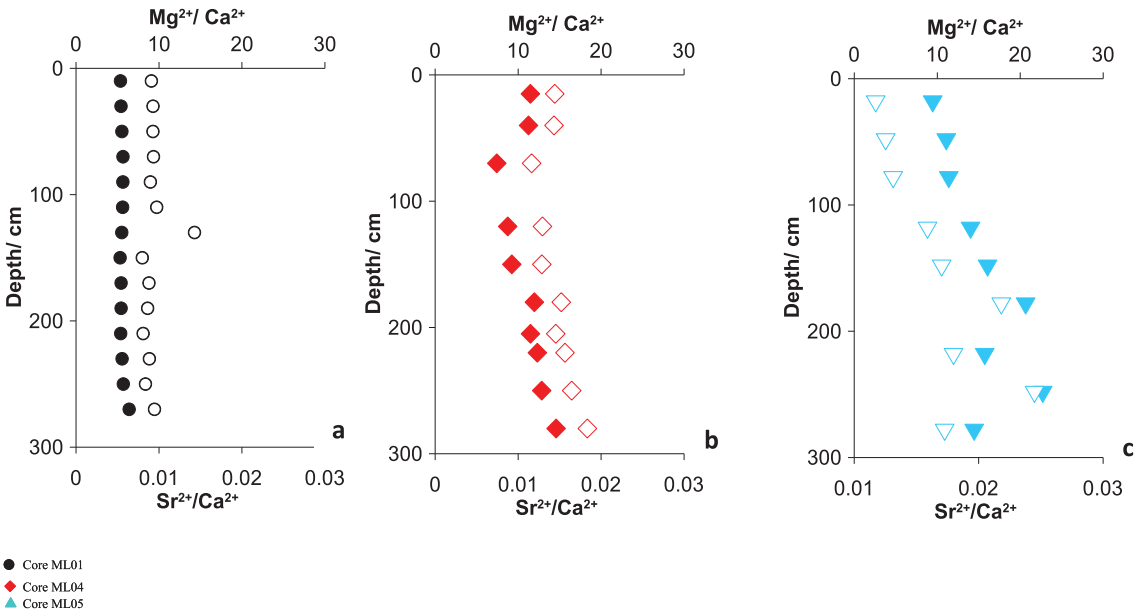

Figure 11. Mg^{2+}/Ca^{2+} (full symbol) and Sr^{2+}/Ca^{2+} (hollow symbol) ratios of the investigated cores.

(Figures 2 and 3). In contrast, pore waters from core ML04 are characterized by high barium concentrations below the SMTZ (Figure 3). A pronounced maximum is observed around 70 cmbsf with values reaching 150 μM. This reflects the dissolution of a barite front just below the SMTZ. A secondary maximum value of 34 μM is also observed at 220 cmbsf and may correspond to the relic of an ancient barite front.

5.6. Seismic Activity and Sulfate Profiles at the North Anatolian Fault: Are They Linked?

This part of our study aims to examine the possible link between the sulfate profiles obtained from our investigated cores and the seismic activity at the two respective gulfs. The chirp-sonar profiles combined with the pore water analyses indicate the presence of gas-bearing sediment in both gulfs. On the other hand, the kink-type sulfate profile for core ML01 with values close to that of seawater over the upper 230 cmbsf means that locally methane does not reach the seafloor: it is entirely consumed by AOM at the SMTZ located deeper. However, such a sulfate profile characterized by a two-step gradient and a SMTZ located at a depth in between 2.5 and 10 mbsf is the most encountered profile type in the Sea of Marmara, especially at sites along the NAF [*Cagatay et al*., 2004; *Halbach et al*., 2004; *Tryon et al*., 2010; *Zitter et al*., 2008]. Therefore, it can be considered as the reference sulfate profile for this seismic area. Such a type of profile was attributed to methane bubbles rising at high rate through the sedimentary column to the seafloor [*Haeckel et al*., 2007]. Thus, methane ebullition is likely responsible for the kink-type sulfate profile commonly encountered along the NAF as a large number of gas plumes have been detected there [*Dupré et al*., 2015]. However, we believe that such a methane ebullition does not currently occur in our sampled sites because the rising rate should be high enough to allow seawater infiltration over few meters depth within the sedimentary column. Assuming that it was the case, this would likely create a plume into the water column detectable on the chirp-sonar profiles, as from previous investigations in this area performed with the same hull mounted profiler [*Gasperini et al*., 2012]. The latter did not detect any evidence of gas plume. In addition to the absence of gas plumes at our sampled sites, it is important to notice that the Gulf of Gemlik area has not experienced large earthquakes ($M_w > 7$) in the recent years, whereas the large 1999 Izmit earthquake in the Gulf of Izmit was reported to release gas from the sediment into the water column [*Kuscu et al*., 2005]. Thus, the rupture of the North Anatolian Fault segment here has likely facilitated the upward movement of methane into the sedimentary column in the Gulf of Izmit [*Kuscu et al*., 2005], leading to its accumulation at the uppermost part. The latter has enhanced the AOM coupled with the precipitation of carbonates at very shallow SMTZ depth, resulting in the depletion of sulfate, calcium, magnesium, and strontium as observed for the cores ML04 and ML05.

Furthermore, Figure 12 summarizes the evolution of the seismicity at both gulfs from the 1999 Izmit earthquake main shock to 2010 [*Karabulut et al*., 2011]. All these seismic data were taken from the seismicity

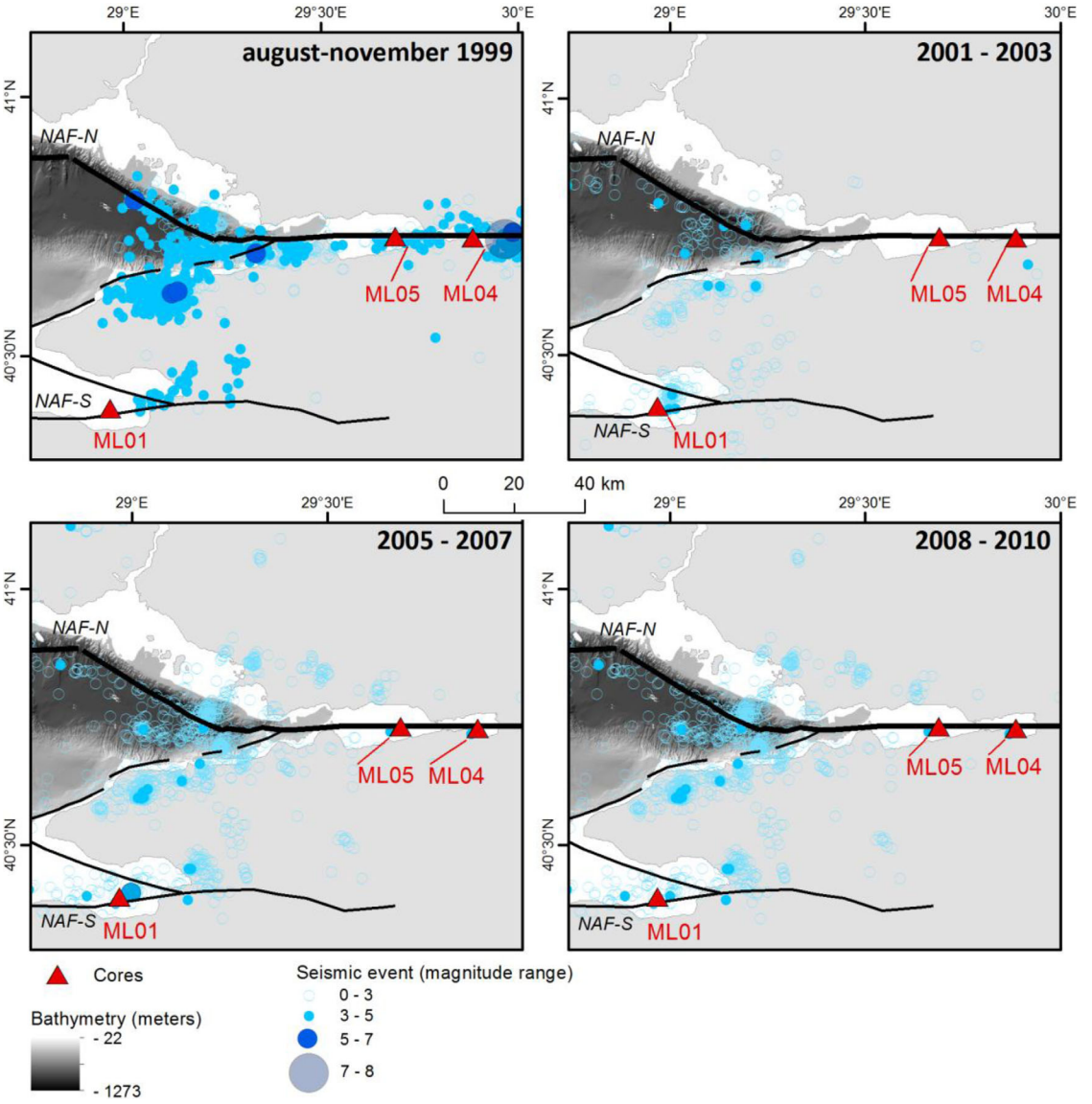

Figure 12. Seismic activity at the Gulfs of Izmit and Gemlik from the 17 August 1999 Izmir earthquake to 2010, seismic data after *Karabulut et al.* [2011]: (a) August to November 1999; (b) 2001–2003; (c) 2005–2007; (d) 2008–2010; and (e) all data.

catalog compiled by *Karabulut et al.* [2011] in order to carry out a spatial analysis (see information herein). The collected data come from station networks of KOERI, IZINET, IPGS, LGTI, CINNET, and TUBITAK, and the recorded seismic events are of magnitude in between 1 and 8. As it was well explained by *Karabulut et al.* [2011], one can clearly see that the seismic activity is very high after the 1999 Izmit earthquake at the two westernmost basins in the Gulf of Izmit where the cores were collected, while a weak activity is recorded in the Gulf of Gemlik. Since this big event, the seismic activity in the Gulf of Izmit considerably decreased to become nearly undetectable from the installed stations, whereas an increasing activity is observed in the GoG with a peak of occurrences at the year interval 2005–2007. The latter is likely related to the $M_w = 5.2$ earthquake which occurred in 2006 in the vicinity of our core site.

Based on all aforementioned elements regarding the type of the sulfate profiles, the SMTZ depth as well as the seismic-activity distribution, we propose the hypothesis that the seismic activity of the areas is a major factor responsible for the transient state of the sulfate profiles by inducing variations in the upward methane flux. In addition, the results of our simulation show that an increase in the methane flux induces a strong perturbation on the sulfate profile which is dissipated within a decade, as the system will return to a new steady state (Figure 10). The fact that methane does not reach the water column for core ML01 while a

$M_w = 5.2$ earthquake has occurred a decade ago (2006) in the area, together with the absence of detectable gas plumes, suggests that only important events like the 1999 Izmit earthquake can trigger intense gas release through faults or strong gas movement from ground shaking. Consequently, this will increase the free methane flux, and give rise to a shoaling of the SMTZ to the very near-seafloor sedimentary layer as observed in Figure 10.

Thus, according to our hypotheses, small to moderate seismic events in the Sea of Marmara would preferentially keep the sulfate profile at transient state while large earthquakes would release large volumes of methane and quickly make the SMTZ evolve to very shallow depth. However in order to validate our hypothesis, more data on pore fluids, gas seeps, and seismicity at key areas along the North Anatolian Fault will be needed over a long period of time. Such an investigation can be part of a long-term monitoring program of seismicity in the Sea of Marmara.

6. Conclusion

The present paper had two goals:

The primary one was to document on pore water geochemistry from cores recovered in the Gulfs of Izmit and Gemlik. The results indicate that the anaerobic oxidation of methane coupled with sulfate reduction occurs at both investigated areas. The results from the core collected in the Gölcük basin revealed the occurrence of barite dissolution beneath the SMTZ and carbonate recrystallization at ~120 cmbsf. The latter has likely precipitated during the reconnection of the easternmost basin of the Sea of Marmara with the Mediterranean Sea.

The second goal of this study was to lay the foundation of possible interrelations between pore water sulfate and the seismic activity in the Marmara region. Therefore, an attempt to explain the shape of the sulfate profiles through the lens of the seismic activity of both gulfs was proposed here. We argued that such an activity is responsible for the kink-type sulfate profile with a fluctuating SMTZ-depth encountered along the North Anatolian Fault. We also speculated that only seismic events characterized by an important energy and methane release can strongly impact on the sulfate concentration, leading to profiles with very shallow SMTZ. This interpretation, although preliminary, offers an interesting route for investigating possible relationships between the spatial distribution of sulfate profile along the North Anatolian Fault, gas seep intensity and the seismic activity at key locations. The temporal aspect would also be contemplated in the frame of long-term monitoring of the North Anatolian Fault.

Acknowledgments

We thank the Captain and the crew of the *R/V* Urania as well as colleagues from both the ITU-Turkey (Dr. Gulsen Ucarkus) and CNR-ISMAR for their technical supports to handle the cores and collect the samples. Pierre Henry is also acknowledged for valuable and constructive comments. Karabulut Hayrullah from the Boğaziçi Universitu-Kandilli Observatory and Earthquake Research Institute, Bohnhoff Marco from GZF-Potsdam, and Schmittbuhl Jean from IPGS are greatly acknowledged for providing the seismic catalogs presented in Figure 10. We appreciate David Fischer and an anonymous reviewer for careful and thorough reviews, which improve the quality of the previous version. Data used in the present paper are from IFREMER and accessible upon request, interested readers can contact the corresponding author Livio Ruffine (livio.ruffine@ifremer.fr).

References

Aloisi, G., M. Drews, K. Wallmann, and G. Bohrmann (2004a), Fluid expulsion from the Dvurechenskii mud volcano (Black Sea): Part I. Fluid sources and relevance to Li, B, Sr, I and dissolved inorganic nitrogen cycles, *Earth Planet. Sci. Lett.*, *225*(3-4), 347–363.

Aloisi, G., K. Wallmann, S. M. Bollwerk, A. Derkachev, G. Bohrmann, and E. Suess (2004b), The effect of dissolved barium on biogeochemical processes at cold seeps, *Geochim. Cosmochim. Acta*, *68*(8), 1735–1748.

Ambraseys, N. (2000), The seismicity of the Marmara Sea area 1800–1899, *J. Earthquake Eng.*, *4*(3), 377–401.

Ambraseys, N. (2001), The earthquake of 1509 in the Sea of Marmara, Turkey, revisited, *Bull. Seismol. Soc. Am.*, *91*(6), 1397–1416.

Ambraseys, N. (2002), The seismic activity of the Marmara Sea region over the last 2000 years, *Bull. Seismol. Soc. Am.*, *92*(1), 1–18.

Ambraseys, N. (2006), Comparison of frequency of occurrence of earthquakes with slip rates from long-term seismicity data: The cases of Gulf of Corinth, Sea of Marmara and Dead Sea Fault Zone, *Geophys. J. Int.*, *165*(2), 516–526.

Ambraseys, N. and J. Jackson (2000), Seismicity of the Sea of Marmara (Turkey) since 1500, *Geophys. J. Int.*, *141*(3), F1–F6.

Armijo, R., et al. (2005), Submarine fault scarps in the Sea of Marmara pull-apart (North Anatolian Fault): Implications for seismic hazard in Istanbul, *Geochem. Geophys. Geosyst.*, *6*, Q06009, doi:10.1029/2004GC000896.

Baker, P. A., M. Kastner, and G. E. Anderson (1981), Mechanism and kinetics of sulfate inhibition on dolomitization of calcium-carbonate, *AAPG Bull.*, *65*(5), 893–894.

Barka, A. (1992), The north Anatolian fault zone, *Ann. Tectonicae*, *VI*, 164–195.

Barka, A. (1999), The 17 August 1999 Izmit earthquake, *Science*, *285*(5435), 1858–1859.

Barka, A. and K. Kadinsky-Cade (1988), Strike-slip fault geometry in Turkey and its influence on earthquake activity, *Tectonics*, *7*(3), 663–684.

Barka, A., et al. (2002), The surface rupture and slip distribution of the 17 August 1999 Izmit earthquake (M 7.4), North Anatolian fault, *Bull. Seismol. Soc. Am.*, *92*(1), 43–60.

Bayon, G., C. Pierre, J. Etoubleau, M. Voisset, E. Cauquil, T. Marsset, N. Sultan, E. Le Drezen, and Y. Fouquet (2007), Sr/Ca and Mg/Ca ratios in Niger Delta sediments: Implications for authigenic carbonate genesis in cold seep environments, *Mar. Geol.*, *241*(1-4), 93–109.

Bayon, G., et al. (2009), Multi-disciplinary investigation of fluid seepage on an unstable margin: The case of the Central Nile deep sea fan, *Mar. Geol.*, *261*(1-4), 92–104.

Berner, R. (1980), *Early Diagenesis: A Theoretical Approach*, Princeton Univ. Press, Princeton, N. J.

Borowski, W. S., C. K. Paull, and W. Ussler (1996), Marine pore-water sulfate profiles indicate in situ methane flux from underlying gas hydrate, *Geology*, *24*(7), 655–658.

Boudreau, B. (1997), *Diagenetic Models and Their Implementation*, 414 pp., Springer-Verlag, Berlin.
Bourry, C., B. Chazallon, J. L. Charlou, J. P. Donval, L. Ruffine, P. Henry, L. Geli, M. N. Cagatay, S. Inan, and M. Moreau (2009), Free gas and gas hydrates from the Sea of Marmara, Turkey Chemical and structural characterization, *Chem. Geol.*, *264*(1-4), 197–206.
Burnard, P., S. Bourlange, P. Henry, L. Geli, M. Tryon, A. Sengör, M. Özeren, and M. Çagatay (2012), Constraints on fluid origins and migration velocities along the Marmara Main Fault (Sea of Marmara, Turkey) using helium isotopes, *Earth Planet. Sci. Lett.*, *341*, 68–78.
Burton, E. A. (1993), Controls on marine carbonate cement mineralogy—Review and reassessment, *Chem. Geol.*, *105*(1-3), 163–179.
Burton, E. A., and L. M. Walter (1987), Relative precipitation rates of aragonite and Mg calcite from seawater—Temperature or carbonate ion control, *Geology*, *15*(2), 111–114.
Cagatay, M. N., N. Gorur, A. Polonia, E. Demirbag, M. Sakinc, M. H. Cormier, L. Capotondi, C. McHugh, O. Emre, and K. Eris (2003), Sea-level changes and depositional environments in the Izmit Gulf, eastern Marmara Sea, during the late glacial-Holocene period, *Mar. Geol.*, *202*(3-4), 159–173.
Cagatay, M. N., M. Ozcan, and E. Gungor (2004), Pore-water and sediment geochemistry in the Marmara Sea (Turkey): Early diagenesis and diffusive fluxes, *Geochem. Explor. Environ. Anal.*, *4*, 213–225.
Cagatay, M. N., et al. (2009), Late Pleistocene-Holocene evolution of the northern shelf of the Sea of Marmara, *Mar. Geol.*, *265*(3-4), 87–100.
Çağatay, M. N., et al. (2012), Sedimentary earthquake records in the İzmit Gulf, Sea of Marmara, Turkey, *Sediment. Geol.*, *282*, 347–359.
Cakir, Z., J. B. de Chabalier, R. Armijo, B. Meyer, A. Barka and G. Peltzer (2003), Coseismic and early post-seismic slip associated with the 1999 Izmit earthquake (Turkey), from SAR interferometry and tectonic field observations, *Geophys. J. Int.*, *155*(1), 93–110.
Cangemi, M., R. Di Leonardo, A. Bellanca, A. Cundy, R. Neri, and M. Angelone (2010), Geochemistry and mineralogy of sediments and authigenic carbonates from the Malta Plateau, Strait of Sicily (Central Mediterranean): Relationships with mud/fluid release from a mud volcano system, *Chem. Geol.*, *276*(3-4), 294–308.
Chuang, P.-C., et al. (2013), Relating sulfate and methane dynamics to geology: Accretionary prism offshore SW Taiwan, *Geochem. Geophys. Geosyst.*, *14*, 2523–2545, doi:10.1002/ggge.20168.
Cormier, M. H., et al. (2006), North Anatolian Fault in the Gulf of Izmit (Turkey): Rapid vertical motion in response to minor bends of a nonvertical continental transform, *J. Geophys. Res.*, *111*, B04102, doi:10.1029/2005JB003633.
Cremiere, A., C. Pierre, M.-M. Blanc-Valleron, T. Zitter, M. N. Cagatay, and P. Henry (2012), Methane-derived authigenic carbonates along the North Anatolian fault system in the Sea of Marmara (Turkey), *Deep Sea Res., Part I*, *66*, 114–130.
Crémière, A., G. Bayon, E. Ponzevera, and C. Pierre (2013), Paleo-environmental controls on cold seep carbonate authigenesis in the Sea of Marmara, *Earth Planet. Sci. Lett.*, *376*, 200–211.
Dupré, S., C. Scalabrin, L. Géli, P. Henry, C. Grall, J.-B. Tary, M. N. Çagatay, and C. Imren (2010), the MARMESONET Scientific Party Team Widespread gas emissions in the Sea of Marmara in relation with the tectonic and sedimentary environments: Results from shipborne multibeam echosounder water column imagery (MARMESONET expedition, 2009), European Geosciences Union General Assembly 2010, 2–7 May, Geophysical Research Abstracts, pp. 9429–9422, Vienna, Austria.
Dupré, S., C. Scalabrin, C. Grall, J. M. Augustin, P. Henry, A. M. C. Şengör, N. Görür, M. N. Çağatay, and L. Géli (2015), Tectonic and sedimentary controls on widespread gas emissions in the Sea of Marmara: Results from systematic, shipborne multibeam echo sounder water column imaging, *J. Geophys. Res. Solid Earth*, *120*, doi:10.1002/2014JB011617, in press.
Embriaco, D., et al. (2014), Monitoring of gas and seismic energy release by multiparametric benthic observatory along the North Anatolian Fault in the Sea of Marmara (NW Turkey), *Geophys. J. Int.*, *196*(2), 850–866.
Ergintav, S., S. McClusky, E. Hearn, R. Reilinger, R. Cakmak, T. Herring, H. Ozener, O. Lenk, and E. Tari (2009), Seven years of postseismic deformation following the 1999, M=7.4 and M=7.2, Izmit-Duzce, Turkey earthquake sequence, *J. Geophys. Res.*, *114*, B07403, doi: 10.1029/2008JB006021.
Eris, K. K., W. B. F. Ryan, M. N. Cagatay, U. Sancar, G. Lericolais, G. Menot, and E. Bard (2007), The timing and evolution of the post-glacial transgression across the Sea of Marmara shelf south of Istanbul, *Mar. Geol.*, *243*(1-4), 57–76.
Eris, K. K., M. N. Cagatay, S. Akcer, L. Gasperini, and Y. Mart (2011), Late glacial to Holocene sea-level changes in the Sea of Marmara: New evidence from high-resolution seismics and core studies, *Geo Mar. Lett.*, *31*(1), 1–18.
Feng, D., and H. H. Roberts (2011), Geochemical characteristics of the barite deposits at cold seeps from the northern Gulf of Mexico continental slope, *Earth Planet. Sci. Lett.*, *309*(1-2), 89–99.
Feng, D., D. Chen, and H. H. Roberts (2009), Petrographic and geochemical characterization of seep carbonate from Bush Hill (GC 185) gas vent and hydrate site of the Gulf of Mexico, *Mar. Pet. Geol.*, *26*(7), 1190–1198.
Fischer, D., J. M. Mogollon, M. Strasser, T. Pape, G. Bohrmann, N. Fekete, V. Spiess, and S. Kasten (2013), Subduction zone earthquake as potential trigger of submarine hydrocarbon seepage, *Nat. Geosci.*, *6*(8), 647–651.
Froelich, P. N., G. Klinkhammer, M. A. A. Bender, N. Luedtke, G. R. Heath, D. Cullen, P. Dauphin, D. Hammond, B. Hartman, and V. Maynard (1979), Early oxidation of organic matter in pelagic sediments of the eastern equatorial Atlantic: Suboxic diagenesis, *Geochim. Cosmochim. Acta*, *43*(7), 1075–1090.
Gasperini, L., and G. Stanghellini (2009), SEISPRHO: An interactive computer program for processing and interpretation of high-resolution seismic reflection profiles, *Comput. Geosci.*, *35*(7), 1497–1507.
Gasperini, L., A. Polonia, G. Bortoluzzi, P. Henry, X. Le Pichon, M. Tryon, N. Cagatay, and L. Geli (2011), How far did the surface rupture of the 1999 Izmit earthquake reach in Sea of Marmara?, *Tectonics*, *30*, TC1010, doi:10.1029/2010TC002726.
Gasperini, L., A. Polonia, F. Del Bianco, G. Etiope, G. Marinaro, P. Favali, F. Italiano, and M. N. Cagatay (2012), Gas seepage and seismogenic structures along the North Anatolian Fault in the eastern Sea of Marmara, *Geochem. Geophys. Geosyst.*, *13*, Q10018, doi:10.1029/2012GC004190.
Géli, L., P. Henry, T. Zitter, S. Dupré, M. Tryon, M. Çagatay, B. de Lépinay, X. Le Pichon, A. Engör, and N. Görür (2008), Gas emissions and active tectonics within the submerged section of the North Anatolian Fault zone in the Sea of Marmara, *Earth Planet. Sci. Lett.*, *274*(1-2), 34–39.
Gieskes, J. M., H. Elderfield, and M. R. Palmer (1986), Strontium and its isotopic composition in interstitial waters of marine carbonate sediments, *Earth Planet. Sci. Lett.*, *77*(2), 229–235.
Goeruer, N., O. Monod, A. I. Okay, C. Sengör, O. Tueysuez, E. Yigitbas, M. Sakinc, and R. Akkoek (1997), Palaeogeographic and tectonic position of the Carboniferous rocks of the western Pontides (Turkey) in the frame of the Variscan belt, *Bull. Soc. Géol. Fr.*, *168*, 197–206.
Gok, E., and O. Polat (2012), An assessment of the seismicity of the Bursa Region from a temporary seismic network, *Pure Appl. Geophys.*, *169*(4), 659–675.
Gorur, N., and M. N. Cagatay (2010), Geohazards rooted from the northern margin of the Sea of Marmara since the late Pleistocene: A review of recent results, *Nat. Hazards*, *54*(2), 583–603.

Haeckel, M., B. P. Boudreau, and K. Wallmann (2007), Bubble-induced porewater mixing: A 3-D model for deep porewater irrigation, *Geochim. Cosmochim. Acta*, *71*(21), 5135–5154.
Halbach, P., E. Holzbecher, T. Reichel, and R. Moche (2004), Migration of the sulphate-methane reaction zone in marine sediments of the Sea of Marmara—Can this mechanism be tectonically induced?, *Chem. Geol.*, *205*(1-2), 73–82.
Hearn, E. H., S. McClusky, S. Ergintav, and R. E. Reilinger (2009), Izmit earthquake postseismic deformation and dynamics of the North Anatolian Fault Zone, *J. Geophys. Res.*, *114*, B08405, doi:10.1029/2008JB006026.
Henkel, S., et al. (2012), Diagenetic barium cycling in Black Sea sediments—A case study for anoxic marine environments, *Geochim. Cosmochim. Acta*, *88*, 88–105.
Hergert, T., and O. Heidbach (2010), Slip-rate variability and distributed deformation in the Marmara Sea fault system, *Nat. Geosci.*, *3*(2), 132–135.
Hergert, T., and O. Heidbach (2011), Geomechanical model of the Marmara Sea region-II. 3-D contemporary background stress field, *Geophys. J. Int.*, *185*(3), 1090–1102.
Hergert, T., O. Heidbach, A. Becel, and M. Laigle (2011), Geomechanical model of the Marmara Sea region-I. 3-D contemporary kinematics, *Geophys. J. Int.*, *185*(3), 1073–1089.
Himmler, T., W. Bach, G. Bohrmann, and J. Peckmann (2010), Rare earth elements in authigenic methane-seep carbonates as tracers for fluid composition during early diagenesis, *Chem. Geol.*, *277*(1-2), 126–136.
Hong, W.-L., M. E. Torres, J.-H. Kim, J. Choi, and J.-J. Bahk (2013), Carbon cycling within the sulfate-methane-transition-zone in marine sediments from the Ulleung Basin, *Biogeochemistry*, *115*(1-3), 129–148.
Hubert-Ferrari, A., A. Barka, E. Jacques, S. S. Nalbant, B. Meyer, R. Armijo, P. Tapponnier, and G. C. P. King (2000), Seismic hazard in the Marmara Sea region following the 17 August 1999 Izmit earthquake, *Nature*, *404*(6775), 269–273.
Irmak, T. S., H. Grosser, M. F. Özer, H. Woith, and S. Barış (2007), The 24 October 2006 Gemlik Earthquake (M = 5.2), paper presented at European Geosciences Union Conference, Vienna.
Karabulut, H., J. Schmittbuhl, S. Ozalaybey, O. Lengline, A. Komec-Mutlu, V. Durand, M. Bouchon, G. Daniel, and M. P. Bouin (2011), Evolution of the seismicity in the eastern Marmara Sea a decade before and after the 17 August 1999 Izmit earthquake, *Tectonophysics*, *510*(1-2), 17–27.
Kasten, S., K. Nöthen, C. Hensen, V. Spieß, M. Blumenberg, and R. R. Schneider (2012), Gas hydrate decomposition recorded by authigenic barite at pockmark sites of the northern Congo Fan, *Geo Mar. Lett.*, *32*, 515–524, doi:10.1007/s00367-012-0288-9.
Kuscu, I., M. Okamura, H. Matsuoka, and Y. Awata (2002), Active faults in the Gulf of Izmit on the North Anatolian Fault, NW Turkey: A high-resolution shallow seismic study, *Mar. Geol.*, *190*(1-2), 421–443.
Kuscu, I., M. Okamura, H. Matsuoka, E. Gokasan, Y. Awata, H. Tur, M. Simsek, and M. Kecer (2005), Seafloor gas seeps and sediment failures triggered by the August 17, 1999 earthquake in the Eastern part of the Gulf of Izmit, Sea of Marmara, NW Turkey, *Mar. Geol.*, *215*(3-4), 193–214.
Kuscu, I., M. Okamura, H. Matsuoka, K. Yamamori, Y. Awata, and S. Ozalp (2009), Recognition of active faults and stepover geometry in Gemlik Bay, Sea of Marmara, NW Turkey, *Mar. Geol.*, *260*(1-4), 90–101.
Kuscu, S. L., P. Halbach, M. Inthorn, T. Kuhn, and R. Seifert (2008), The R/V Meteor cruise leg M44/1 in February 1999 in the Sea of Marmara: The first multibeam bathymetric study and analysis of methane in sediment and water columns, *Turk. J. Earth Sci.*, *17*(3), 461–480.
Langridge, R. M., H. D. Stenner, T. E. Fumal, S. A. Christofferson, T. K. Rockwell, R. D. Hartleb, J. Bachhuber, and A. A. Barka (2002), Geometry, slip distribution, and kinematics of surface rupture on the Sakarya fault segment during the 17 August 1999 Izmit, Turkey, earthquake, *Bull. Seismol. Soc. Am.*, *92*(1), 107–125.
Lapham, L. L., M. Alperin, J. Chanton, and C. Martens (2008), Upward advection rates and methane fluxes, oxidation, and sources at two Gulf of Mexico brine seeps, *Mar. Chem.*, *112*(1-2), 65–71.
Le Pichon, X., et al. (2001), The active Main Marmara Fault, *Earth Planet. Sci. Lett.*, *192*(4), 595–616.
Le Pichon, X., N. Chamotrooke, C. Rangin, and A. M. C. Sengor (2003), The North Anatolian fault in the Sea of Marmara, *J. Geophys. Res.*, *108*(B4), 2179, doi:10.1029/2002JB001862.
McHugh, C. M. G., L. Seeber, M. H. Cormier, J. Dutton, N. Cagatay, A. Polonia, W. B. F. Ryan, and N. Gorur (2006), Submarine earthquake geology along the North Anatolia Fault in the Marmara Sea, Turkey: A model for transform basin sedimentation, *Earth Planet. Sci. Lett.*, *248*(3-4), 661–684.
McHugh, C. M. G., D. Gurung, L. Giosan, W. B. F. Ryan, Y. Mart, U. Sancar, L. Burckle, and M. N. Cagatay (2008), The last reconnection of the Marmara Sea (Turkey) to the World Ocean: A paleoceanographic and paleoclimatic perspective, *Mar. Geol.*, *255*(1-2), 64–82.
Meade, B. J., B. H. Hager, S. C. McClusky, R. E. Reilinger, S. Ergintav, O. Lenk, A. Barka, and H. Ozener (2002), Estimates of seismic potential in the Marmara Sea region from block models of secular deformation constrained by global positioning system measurements, *Bull. Seismol. Soc. Am.*, *92*(1), 208–215.
Meister, P., B. Liu, T. G. Ferdelman, B. B. Jørgensen, and A. Khalili (2013), Control of sulphate and methane distributions in marine sediments by organic matter reactivity, *Geochim. Cosmochim. Acta*, *104*, 183–193.
Moore, T. S., R. W. Murray, A. C. Kurtz, and D. P. Schrag (2004), Anaerobic methane oxidation and the formation of dolomite, *Earth Planet. Sci. Lett.*, *229*(1-2), 141–154.
Niewohner, C., C. Hensen, S. Kasten, M. Zabel, and H. D. Schulz (1998), Deep sulfate reduction completely mediated by anaerobic methane oxidation in sediments of the upwelling area off Namibia, *Geochim. Cosmochim. Acta*, *62*(3), 455–464.
Noethen, K., and S. Kasten (2011), Reconstructing changes in seep activity by means of pore water and solid phase Sr/Ca and Mg/Ca ratios in pockmark sediments of the Northern Congo Fan, *Mar. Geol.*, *287*(1-4), 1–13.
Pierre, C., M. M. Blanc-Valleron, J. Demange, O. Boudouma, J. P. Foucher, T. Pape, T. Himmler, N. Fekete, and V. Spiess (2012), Authigenic carbonates from active methane seeps offshore southwest Africa, *Geo Mar. Lett.*, *32*, 501–513, doi:10.1007/s00367-012-0295-x.
Polonia, A., et al. (2004), Holocene slip rate of the North Anatolian Fault beneath the Sea of Marmara, *Earth Planet. Sci. Lett.*, *227*(3–4), 411–426.
Pondrelli, S., S. Salimbeni, A. Morelli, G. Ekström, L. Postpischl, G. Vannucci, and E. Boschi (2011), European–Mediterranean regional centroid moment tensor catalog: Solutions for 2005–2008, *Phys. Earth Planet. Inter.*, *185*(3), 74–81.
Reeburgh, W. S. (1976), Methane consumption in Cariaco Trench waters and sediments, *Earth Planet. Sci. Lett.*, *28*(3), 337–344.
Regnier, P., A. W. Dale, S. Arndt, D. LaRowe, J. Mogollon, and P. Van Cappellen (2011), Quantitative analysis of anaerobic oxidation of methane (AOM) in marine sediments: A modeling perspective, *Earth Sci. Rev.*, *106*, 105–130, doi:10.1016/j.earscirev.2011.01.002.
Reichel, T., and P. Halbach (2007), An authigenic calcite layer in the sediments of the Sea of Marmara—A geochemical marker horizon with pale oceanographic significance, *Deep Sea Res., Part II*, *54*(11-13), 1201–1215.

Reilinger, R., et al. (2006), GPS constraints on continental deformation in the Africa-Arabia-Eurasia continental collision zone and implications for the dynamics of plate interactions, *J. Geophys. Res.*, *111*, B05411, doi:10.1029/2005JB004051.

Ruffine, L., et al. (2012), Geochemical dynamics of the natural-gas hydrate system in the Sea of Marmara, offshore Turkey, in *Advances in Natural Gas Technology*, pp. 29–56, InTech, Rijeka-Croatia.

Scholz, F., C. Hensen, A. Reitz, R. L. Romer, V. Liebetrau, A. Meixner, S. M. Weise, and M. Haeckel (2009), Isotopic evidence (Sr-87/Sr-86, delta Li-7) for alteration of the oceanic crust at deep-rooted mud volcanoes in the Gulf of Cadiz, NE Atlantic Ocean, *Geochim. Cosmochim. Acta*, *73*(18), 5444–5459.

Seeberg-Elverfeldt, J., M. Schlüter, T. Feseker, and M. Kölling (2005), Rhizon sampling of pore waters near the sediment/water interface of aquatic systems, *Limnol. Oceanogr. Methods*, *3*, 361–371.

Sengor, A. M. C., O. Tuysuz, C. Imren, M. Sakinc, H. Eyidogan, G. Gorur, X. Le Pichon, and C. Rangin (2005), The North Anatolian Fault: A new look, *Annual Review of Earth and Planetary Sciences*, pp. 37–112.

Snyder, G. T., A. Hiruta, R. Matsurnoto, G. R. Dickens, H. Tomaru, R. Takeuchi, J. Komatsubara, Y. Ishida, and H. Yu (2007), Pore water profiles and authigenic mineralization in shallow marine sediments above the methane-charged system on Umitaka Spur, Japan Sea, *Deep Sea Res., Part II*, *54*, 1216–1239.

Solomon, E. A., and M. Kastner (2012), Progressive barite dissolution in the Costa Rica forearc—Implications for global fluxes of Ba to the volcanic arc and mantle, *Geochim. Cosmochim. Acta*, *83*, 110–124.

Tanircan, G., and N. Savas (2011), Strong ground motion simulation by the Empirical Green's Function method for Bursa-Yalova Region, Turkey, *Bull. Earthquake Eng.*, *9*(5), 1327–1338.

Tary, J. B., L. Geli, C. Guennou, P. Henry, N. Sultan, N. Cagatay, and V. Vidal (2012), Microevents produced by gas migration and expulsion at the seabed: A study based on sea bottom recordings from the Sea of Marmara, *Geophys. J. Int.*, *190*(2), 993–1007.

Tryon, M. D., P. Henry, M. N. Cagatay, T. A. C. Zitter, L. Geli, L. Gasperini, P. Burnard, S. Bourlange, and C. Grall (2010), Pore fluid chemistry of the North Anatolian Fault Zone in the Sea of Marmara: A diversity of sources and processes, *Geochem. Geophys. Geosyst.*, *11*, Q0AD03, doi:10.1029/2010GC003177.

Ucarkus, G., Z. Cakir, and R. Armijo (2011), Western termination of the Mw 7.4, 1999 Izmit earthquake rupture: Implications for the expected large earthquake in the Sea of Marmara, *Turk. J. Earth Sci.*, *20*(4), 379–394.

Ussler, W., III, C. Paull, and P. Fullagar (2000), Pore-water Strontium isotopes from the Leg 171B drilling transect down the Blake Spur., *Proc. Ocean Drill. Program, Sc. Res.*, vol. 171B.

Vanneste, H., M. Kastner, R. H. James, D. P. Connelly, R. E. Fisher, B. A. Kelly-Gerreyn, K. Heeschen, M. Haeckel, and R. A. Mills (2012), Authigenic carbonates from the Darwin Mud Volcano, Gulf of Cadiz: A record of palaeo-seepage of hydrocarbon bearing fluids, *Chem. Geol.*, *300*, 24–39.

Vidal, L., G. Menot, C. Joly, H. Bruneton, F. Rostek, M. N. Cagatay, C. Major, and E. Bard (2010), Hydrology in the Sea of Marmara during the last 23 ka: Implications for timing of Black Sea connections and sapropel deposition, *Paleoceanography*, *25*, PA1205, doi:10.1029/2009PA001735.

Wallmann, K., M. Drews, G. Aloisi, and G. Bohrmann (2006a), Methane discharge into the Black Sea and the global ocean via fluid flow through submarine mud volcanoes, *Earth Planet. Sci. Lett.*, *248*(1-2), 545–560.

Wallmann, K., G. Aloisi, M. Haeckel, A. Obzhirov, G. Pavlova, and P. Tishchenko (2006b), Kinetics of organic matter degradation, microbial methane generation, and gas hydrate formation in anoxic marine sediments, *Geochim. Cosmochim. Acta*, *70*(15), 3905–3927.

Whiticar, M. J. (1999), Carbon and hydrogen isotope systematics of bacterial formation and oxidation of methane, *Chem. Geol.*, *161*(1-3), 291–314.

Whiticar, M. J. and E. Faber (1986), Methane oxidation in sediment and water column environments—Isotope evidence, *Org. Geochem.*, *10*(4-6), 759–768.

Wilson, R. M., L. Macelloni, A. Simonetti, L. Lapham, C. Lutken, K. Sleeper, M. D'Emidio, M. Pizzi, J. Knapp, and J. Chanton (2014), Subsurface methane sources and migration pathways within a gas hydrate mound system, Gulf of Mexico, *Geochem. Geophys. Geosyst.*, *15*(1), 89–107.

Yalciner, A. C., B. Alpar, Y. Altinok, I. Ozbay, and F. Imamura (2002), Tsunamis in the Sea of Marmara—Historical documents for the past, models for the future, *Mar. Geol.*, *190*(1-2), 445–463.

Yoshinaga, M. Y., T. Holler, T. Goldhammer, G. Wegener, J. W. Pohlman, B. Brunner, M. M. M. Kuypers, K.-U. Hinrichs, and M. Elvert (2014), Carbon isotope equilibration during sulphate-limited anaerobic oxidation of methane, *Nat. Geosci.*, *7*(3), 190–194.

Zitter, T., P. Henry, G. Aloisi, G. Delaygue, M. Çagatay, B. Mercier de Lepinay, M. Al-Samir, F. Fornacciari, M. Tesmer, and A. Pekdeger (2008), Cold seeps along the main Marmara fault in the Sea of Marmara (Turkey), *Deep Sea Res., Part I*, *55*(4), 552–570.